PLOS GENETICS

RESEARCH ARTICLE

Actin assembly and non-muscle myosin activity drive dendrite retraction in an UNC-6/Netrin dependent self-avoidance response

Lakshmi Sundararajan[1], Cody J. Smith[1¤a], Joseph D. Watson[2¤b], Bryan A. Millis[1,3,4], Matthew J. Tyska[1], David M. Miller, III[1,2]*

1 Department of Cell and Developmental Biology, Vanderbilt University, Nashville, Tennessee, United States of America, **2** Neuroscience Graduate Program, Vanderbilt University, Nashville, Nashville, Tennessee, United States of America, **3** Cell Imaging Shared Resource, Vanderbilt University, Nashville, Nashville, Tennessee, United States of America, **4** Vanderbilt Biophotonics Center, Vanderbilt University, Nashville, Nashville, Tennessee, United States of America

¤a Current address: Department of Biological Sciences, Notre Dame University, South Bend, Indiana, United States of America
¤b Current address: Rho, Chapel Hill, North Carolina, United States of America
* david.miller@vanderbilt.edu

Citation: Sundararajan L, Smith CJ, Watson JD, Millis BA, Tyska MJ, Miller DM, III (2019) Actin assembly and non-muscle myosin activity drive dendrite retraction in an UNC-6/Netrin dependent self-avoidance response. PLoS Genet 15(6): e1008228. https://doi.org/10.1371/journal.pgen.1008228

Editor: Bing Ye, University of Michigan, UNITED STATES

Received: April 26, 2019

Accepted: June 4, 2019

Published: June 20, 2019

Data Availability Statement: All relevant data are within the manuscript and its Supporting Information files.

Funding: This work was supported by NIH Grants R01 NS079611 to DMM, F31 NS071801 to CJS and F31 NS49743 to JDW. Some of the strains used in this work were provided by the C. elegans Genetics Center, which is supported by the US National Institutes of Health (NIH) National Center for Research Resources. The funders had no role

Abstract

Dendrite growth is constrained by a self-avoidance response that induces retraction but the downstream pathways that balance these opposing mechanisms are unknown. We have proposed that the diffusible cue UNC-6(Netrin) is captured by UNC-40(DCC) for a short-range interaction with UNC-5 to trigger self-avoidance in the *C. elegans* PVD neuron. Here we report that the actin-polymerizing proteins UNC-34(Ena/VASP), WSP-1(WASP), UNC-73(Trio), MIG-10(Lamellipodin) and the Arp2/3 complex effect dendrite retraction in the self-avoidance response mediated by UNC-6(Netrin). The paradoxical idea that actin polymerization results in shorter rather than longer dendrites is explained by our finding that NMY-1 (non-muscle myosin II) is necessary for retraction and could therefore mediate this effect in a contractile mechanism. Our results also show that dendrite length is determined by the antagonistic effects on the actin cytoskeleton of separate sets of effectors for retraction mediated by UNC-6(Netrin) versus outgrowth promoted by the DMA-1 receptor. Thus, our findings suggest that the dendrite length depends on an intrinsic mechanism that balances distinct modes of actin assembly for growth versus retraction.

Author summary

Neurons may extend highly branched dendrites to detect input over a broad receptive field. The formation of actin filaments may drive dendrite elongation. The architecture of the dendritic arbor also depends on mechanisms that limit expansion. For example, sister dendrites from a single neuron usually do not overlap due to self-avoidance. Although cell surface proteins are known to mediate self-avoidance, the downstream pathways that drive dendrite retraction in this phenomenon are largely unknown. Studies of the highly

in study design, data collection and analysis, decision to publish, or preparation of the manuscript.

Competing interests: The authors have declared that no competing interests exist.

branched PVD sensory neuron in *C. elegans* have suggested a model of self-avoidance in which the UNC-40/DCC receptor captures the diffusible cue UNC-6/Netrin at the tips of PVD dendrites where it interacts with the UNC-5 receptor on an opposing sister dendrite to induce retraction. Here we report genetic evidence that UNC-5-dependent retraction requires downstream actin polymerization. This finding evokes a paradox: How might actin polymerization drive both dendrite growth and retraction? We propose two answers: (1) Distinct sets of effectors are involved in actin assembly for growth vs retraction; (2) Non-muscle myosin interacts with a nascent actin assemblage to trigger retraction. Our results show that dendrite length depends on the balanced effects of specific molecular components that induce growth vs retraction.

Introduction

Dendritic arbors are defined by the balanced effects of outgrowth which expands the structure versus retraction which constrains the size of the receptive field. Microtubules and filamentous actin (F-actin) are prominent dendritic components and have been implicated as key drivers of dendritic growth and maintenance by the finding that treatments that perturb cytoskeletal dynamics may also disrupt dendritic structure [1–3]. For many neurons, dendritic growth is highly exuberant with multiple tiers of branches projecting outward from the cell soma. Ultimately, growth may be terminated by external cues. For example, neurons with similar functions are typically limited to separate domains by tiling mechanisms in which mutual contact induces dendrite retraction. Similarly, the related phenomenon of self-avoidance is widely observed to prevent overlaps among sister dendrites arising from a single neuron [4]. Homotypic interactions between the membrane components Dscam and protocaderins can mediate the self-avoidance response [5–7]. Surprisingly, in some instances, soluble axon guidance cues and their canonical receptors are also required. For example, self-avoidance for the highly-branched Purkinje neuron depends on both protocadherins and also repulsive interactions between sister dendrites decorated with the Robo receptor and its diffusible ligand, Slit [8]. In another example, we have shown that UNC-6/Netrin and its cognate receptors, UNC-5 and UNC-40/DCC, mediate self-avoidance for PVD nociceptive neurons in *C. elegans* [9]. Although multiple cell-surface interactions are now known to trigger self-avoidance, downstream effectors that drive dendrite retraction in this mechanism are poorly understood.

The PVD neurons, one on each side of the body, build complex dendritic arbors through a series of successive 1˚, 2˚, 3˚ and 4˚ orthogonal branching events [10] [11–13]. Self-avoidance ensures that adjacent 3˚ branches do not overgrow one another [9,11] (S1 Fig). Our previous results suggested a novel mechanism of self-avoidance in which UNC-40/DCC captures UNC-6/Netrin at the PVD cell surface and then triggers retraction by interacting with UNC-5 on the neighboring 3^{o} branch. UNC-40/DCC may also effect self-avoidance by acting in a separate pathway that does not involve UNC-6/Netrin [9]. Here we describe a cell biological model of dendrite retraction in the PVD self-avoidance response that depends on actin polymerization.

The structure of the actin cytoskeleton is controlled by a wide array of effector proteins that regulate specific modes of actin polymerization. For example, Ena/VASP enhances F-actin elongation at the plus-end [12] and the Arp2/3 complex functions with WASP (Wiskott-Aldrich syndrome protein) and the Wave Regulatory Complex (WRC) to promote F-actin branching [13]. Upstream regulators of WASP and the WRC include Rho family GTPases [14] and their activators, the GEFs (Guanine nucleotide Exchange Factors) UNC-73/Trio [15,16] and TIAM (T-cell Lymphoma Invasion and Metastasis Factor) [17,18]. Members of the

Lamellipodin/Lpd family recruit Ena/VASP to localize F-actin assembly at the leading edge of migrating cells [19]. The fact that all of these components (UNC-34/Ena/VASP, Arp2/3 complex, WSP-1/WASP, WRC, UNC-73/Trio, TIAM/TIAM-1, MIG-10/lamellipodin) have been previously shown to function in *C. elegans* to mediate axon guidance underscores the key role of the actin cytoskeleton in growth cone steering [15,18,20–23].

Our results show that UNC-34/Ena/VASP functions downstream of UNC-5 to mediate PVD self-avoidance. Genetic evidence detecting roles for the Arp2/3 complex and its upstream regulator, WASP/WSP-1, indicates that the formation of branched actin networks may contribute to dendrite retraction. A necessary role for actin polymerization is also indicated by the defective PVD self-avoidance response of mutants with disabled UNC-73/Trio or MIG-10/lamellipodin. We show that PVD self-avoidance also requires NMY-1/non-muscle myosin II which we propose effects dendrite retraction in a contractile mechanism that drives the reorganization of the nascent actin cytoskeleton. The necessary role for myosin could explain how actin polymerization can result in shorter rather than longer dendrites in the self-avoidance response. Thus, we propose that UNC-6/Netrin triggers self-avoidance by simultaneously stimulating actin assembly and non-muscle myosin activity in 3˚ dendrites.

Because dendrite growth depends on actin polymerization [24,25], our finding that the actin cytoskeleton is also necessary for dendrite self-avoidance points to different modes of actin polymerization for growth *vs* retraction. Recent work has shown that a multicomponent complex involving the PVD membrane proteins DMA-1 and HPO-30 drives dendritic growth by linking the PVD actin cytoskeleton to adhesive cues on the adjacent epidermis [26,27]. Dendrite elongation, in this case, depends on the WRC and TIAM-1, both of which are known to promote actin polymerization. In contrast, our work has revealed that effectors of actin polymerization that are required for 3˚ branch self-avoidance (e.g., UNC-34/Ena/VASP, MIG-10/lamellipodin, UNC-73/Trio, Arp2/3 complex, WSP-1/WASP) are not necessary for 3˚ dendrite outgrowth. Additionally, we show that UNC-6/Netrin signaling antagonizes the DMA-1-dependent mechanism of dendritic growth. These findings are significant because they suggest that overall dendrite length is defined by the relative strengths of opposing pathways that utilize separate sets of effectors to differentially regulate actin polymerization for either growth or retraction.

Results

UNC-6/Netrin mediates PVD sister dendrite self-avoidance

To visualize PVD morphology, we utilized a previously characterized GFP marker driven by a PVD-specific promoter (*PVD*::GFP) (S1A and S1B Fig)[11]. Each PVD neuron adopts a stereotypical morphology characterized by a series of orthogonal junctions between adjacent branches: 1˚ dendrites extend laterally from the PVD cell soma; each 2˚ dendrite projects along the dorsal-ventral axis to generate a T-shaped junction comprised of two 3˚ dendrites each with either an anterior or posterior trajectory; terminal 4˚ dendrites occupy interstitial locations between the epidermis and body muscles. The net result of this branching pattern is a series of tree-like structures or menorahs distributed along the 1˚ dendrite. In contrast to the highly branched dendritic architecture, a single axon projects from the PVD cell soma to join the ventral nerve cord [10,11,26]. Despite the complexity of this network, dendrites rarely overlap (< 5%) in the mature PVD neuron (S1A Fig) [9]. Self-avoidance depends on an active process in which sister PVD dendrites retract upon physical contact with one another (S1C Fig). In the wild type, 3˚ branches arising from adjacent menorahs initially grow outward toward one another but then retract after mutual contact. The net result is a characteristic gap between the tips of 3˚ dendrites in neighboring menorahs [11]. We have previously shown

that 3˚ dendrite self-avoidance depends in part on the diffusible cue UNC-6/Netrin and its canonical receptors, UNC-40/DCC and UNC-5 [9]. Mutations that disable *unc-6*, for example, result in a significant increase in the fraction of 3˚ dendrites that fail to retract and remain in contact (S1B Fig, Fig 3D). Similar self-avoidance defects were observed for mutants of either *unc-40* or *unc-5*. Our results are consistent with a model in which UNC-40 captures UNC-6 for contact with UNC-5 at the tips of adjacent 3˚ dendrites (S1D Fig) [9]. Here we address the question of how the activated UNC-5 receptor then modifies the actin cytoskeleton to drive dendrite retraction.

Constitutively active UNC-5 delays dendrite outgrowth

We have proposed that UNC-6 initiates dendrite retraction by activating UNC-5 [9]. This model predicts that a constitutively active form of UNC-5 should retard net outgrowth of 3˚ dendrites by triggering an opposing retraction mechanism. To test this idea, we attached a myristoylation sequence to the cytoplasmic domain of UNC-5 [27]. The resultant myristyolated UNC-5 intracellular domain (MYR::UNC-5) is effectively tethered to the cytoplasmic membrane which is sufficient to activate UNC-5-dependent downstream signaling [27]. Expression of MYR::UNC-5 in PVD results in substantially shorter 3˚ dendrites in comparison to wild type at the L3 stage (Fig 1A–1C). This phenotype suggests that constitutive activation of UNC-5 impairs normal outgrowth of 3˚ dendrites. We tested this idea by scoring the dynamic status of 3˚ dendrites. To quantify movement, we measured the distance from a fiduciary point to the tip of a 3˚ dendrite at intervals over time (delta t = 240 sec) (Fig 1E) (S1 and S2 Movies). Examples of these measurements are shown in Fig 1E. We observed that wild-type 3˚ dendrites typically display saltatory movement with periodic bouts of extension and retraction that result in net elongation. In contrast, 3˚ dendrites of PVD neurons expressing MYR::UNC-5 grow more slowly and rarely show periods of active extension and retraction (Fig 1E and 1F). The higher overall motility of 3˚ dendrites in the wild type vs PVD::MYR::UNC-5 is evident from a comparison of the standard deviation of the net movement of 3˚ dendrites in each strain (Fig 1F). Despite slower outgrowth, 3˚ dendrites expressing MYR::UNC-5 eventually produce a normal-appearing PVD architecture by the late L4 stage (Fig 2A). MYR::UNC-5 lacks the extracellular UNC-6-binding domain (Fig 1D) and thus should function independently of UNC-6. We confirmed this prediction by demonstrating that MYR::UNC-5 prevents the self-avoidance defect observed in an *unc-6* mutant in L4 stage animals (Fig 2B–2D). We attribute this effect to the constitutive activation of dendrite retraction by MYR::UNC-5 that effectively prevents overgrowth of adjacent sister 3˚ dendrites in an *unc-6/Netrin* mutant. Together, these results are consistent with the hypothesis that UNC-5 functions downstream of UNC-6/Netrin to trigger dendrite retraction in the self-avoidance response. Given the well-established role of UNC-5 as an UNC-6/Netrin receptor [28,29], we favor this model over the alternative hypothesis that UNC-5 functions in parallel to UNC-6/Netrin which is also consistent with these epistasis results.

UNC-34/Ena/VASP mediates self-avoidance in actin-containing PVD dendrites

To explore potential modifications of the PVD cytoskeleton as effectors of the UNC-6/Netrin-dependent self-avoidance response, we used live cell markers to visualize actin (PVD::ACT-1::GFP) and microtubules (*pdes-2*::TBA-1::mCherry) in PVD [30]. We observed a robust ACT-1::GFP signal throughout the PVD neuron including the axon and all dendrites (Fig 3A). In contrast, the TBA-1::mCherry signal was strongest in the PVD axon and 1˚ dendrite. This result confirms an earlier report suggesting that dendritic microtubules are most abundant in

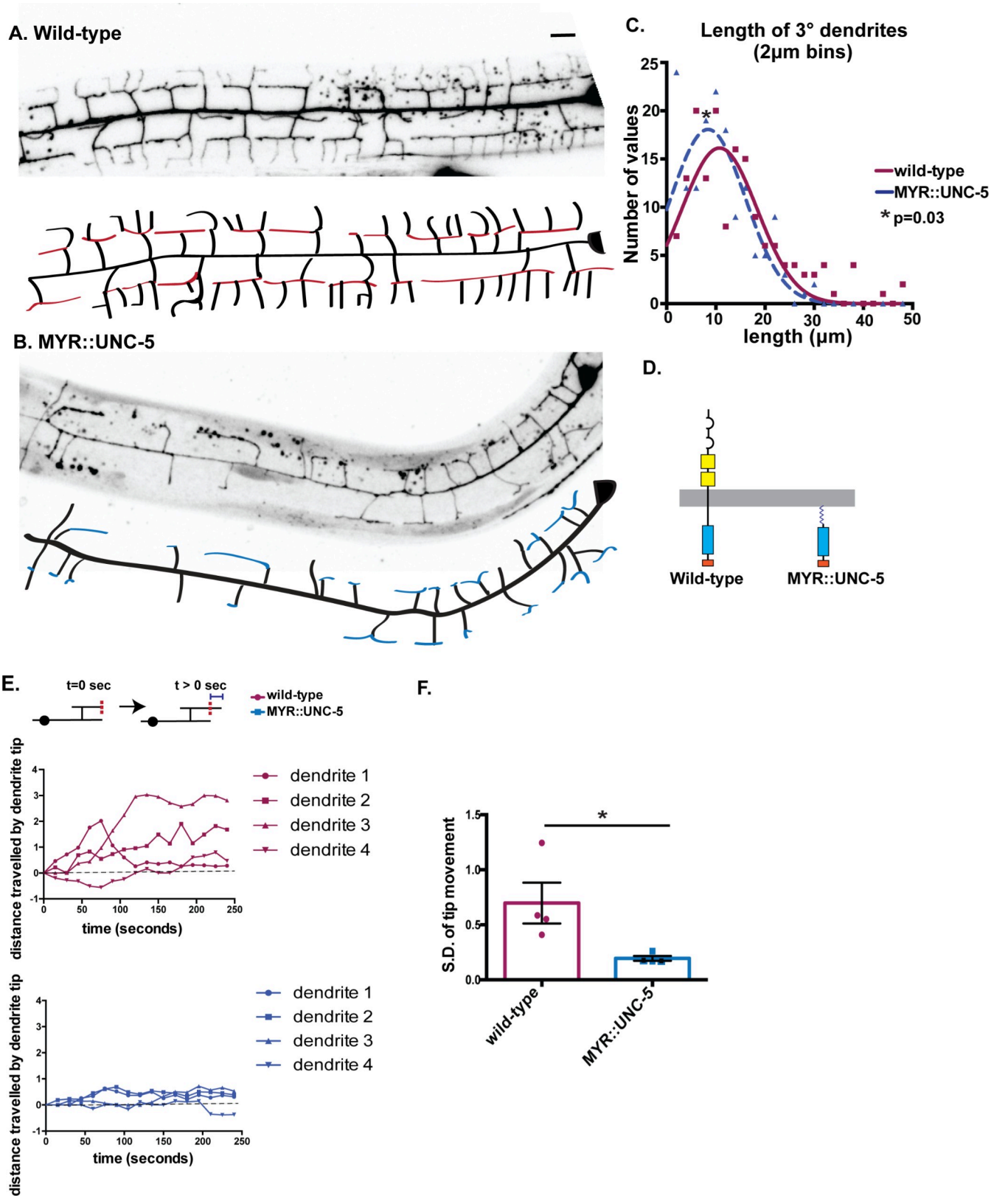
A. Wild-type
B. MYR::UNC-5
C.
Length of 3° dendrites
(2µm bins)
Number of values
length (µm)
wild-type
MYR::UNC-5
* p=0.03
D.
Wild-type
MYR::UNC-5
E.
t=0 sec
t > 0 sec
wild-type
MYR::UNC-5
distance travelled by dendrite tip
time (seconds)
dendrite 1
dendrite 2
dendrite 3
dendrite 4
F.
S.D. of tip movement
wild-type
MYR::UNC-5

Fig 1. Constitutively active UNC-5 retards outgrowth of 3˚ PVD dendrites. (A-D) Representative images and tracings of 3˚ dendrites anterior to PVD cell body in (A) wild type (red) and (B) PVD::MYR::UNC-5 (blue) (Late L3-early L4 animals) (C) Gaussian fit to distribution of lengths of PVD::mCherry-labeled 3˚ dendrites showing shorter average length for MYR::UNC-5 (n = 156, 7 animals) *versus* wild type (n = 159, 8 animals), p = 0.03, Kolmogorov-Smirnov statistical test. (D) Schematics of intact, wild-type UNC-5 receptor vs membrane-associated, constitutively-activated myristylated-UNC-5 (MYR::MYR-5). (E-F) Dynamicity of 3˚ dendrites in wild-type vs MYR::UNC-5-expressing PVD neurons labeled with PVD::GFP. (E) Schematic (top) depicts displacement of the tip of a 3˚ dendrite relative to a fiduciary mark (vertical dashed red line). Scale bar is 10 μm. Representative plots of displacement for wild-type (red) and MYR::UNC-5 (blue) 3˚ dendrites over time. (F) The dynamic saltatory growth and retraction of 3˚ dendrites in the wild type vs the relative quiescence of MYR::UNC-5-expressing PVD neurons is correlated with elevated standard deviation of tip movement from a fiduciary point in wild-type vs MYR::UNC-5 expressing PVD neurons (p = 0.04 from Student's t-test. n = 4).

https://doi.org/10.1371/journal.pgen.1008228.g001

the 1˚ branch (Fig 3A) [30]. We thus considered the possibility that the self-avoidance response could depend on the regulation of actin dynamics. To test this idea, we examined the PVD self-avoidance phenotype for a mutation that disables the actin binding protein, Ena/VASP. We selected Ena/VASP for this test because it has been shown to function as a cytoplasmic effector of actin polymerization downstream of *unc-6/Netrin* signaling [12,31,32]. In addition, the *C. elegans* Ena/VASP homolog, UNC-34 [33], is enriched in a gene expression profile of PVD neurons [11]. A strong loss-of-function allele of *unc-34*/Ena/VASP [34] alters overall PVD morphology (e.g., truncated or misplaced 1˚ dendrite, fewer 2˚ branches) (Fig 3B and 3C, S2A–S2C Fig). In contrast, mutations in other regulators of actin polymerization (e.g. TIAM-1/Gef, S2D Fig) result in severe truncation of lateral branches including 3˚ dendrites, a phenotype that points to a role for actin polymerization in dendrite outgrowth [24,25]. PVD neurons in *unc-34* mutant animals show the opposite effect of adjacent 3˚ dendrites that fail to self-avoid and overgrow one another (Fig 3B and 3C). PVD-specific expression of mCherry-tagged UNC-34 protein rescued this Unc-34 mutant phenotype suggesting that *unc-34* function is cell-autonomous for the self-avoidance response (Fig 3C). *unc-34* mutant 1˚ and 2˚ branch defects were not rescued by PVD expression of UNC-34, however, which could be indicative of an additional UNC-34 function in nearby cell types that influence PVD morphogenesis (Fig 3B, S2 Fig) [35,36]. Thus, our results suggest that UNC-34/Ena/VASP is selectively required in PVD neurons for dendrite retraction in the self-avoidance response but not for dendrite outgrowth. The previously established role of UNC-34/Ena/VASP as a downstream effector of UNC-5 [20] predicts that *unc-34* should be epistatic to the MYR::UNC-5 gain-of-function phenotype. We confirmed this prediction by showing that the delayed outgrowth PVD dendrites in the PVD::MYR::UNC-5 strain is fully suppressed in *unc-34* mutant backgrounds which display the Unc-34 self-avoidance defect (Fig 3C). This result stands in striking contrast to our finding above that PVD::MYR::UNC-5 is epistatic to the Unc-6 self-avoidance phenotype (Fig 2B–2D). Thus, our genetic results are consistent with a model in which UNC-6/Netrin acts through UNC-5 to activate UNC-34/Ena/VASP for dendrite retraction in the self-avoidance response.

For visualizing UNC-34/Ena/VASP in developing dendrites, we labeled UNC-34 with mCherry and co-expressed it in PVD (PVD::mCherry::UNC-34) with LifeAct::GFP to detect actin-containing structures. mCherry::UNC-34 is functional because it rescues the *unc-34* self-avoidance defect (Fig 3C). iSIM super resolution imaging detected punctate mCherry::UNC-34 throughout the PVD dendritic array (Fig 4A and 4B). Additional images collected by AiryScan microscopy also detected punctate mCherry::UNC-34 in PVD dendrites (S3 Fig, S1 Methods). Notably, mCherry::UNC-34 puncta are consistently detected at the tips of 3˚ dendrites (Fig 4A–4C, S3A and S3B Fig), a finding that parallels the observed distal location of Ena/VASP in F-actin containing filopodial structures [37,38]. Our results are thus consistent with the idea that UNC-34/Ena/VASP functions at the tips of 3˚ dendrites mediate actin assembly for branch retraction in the self-avoidance response.

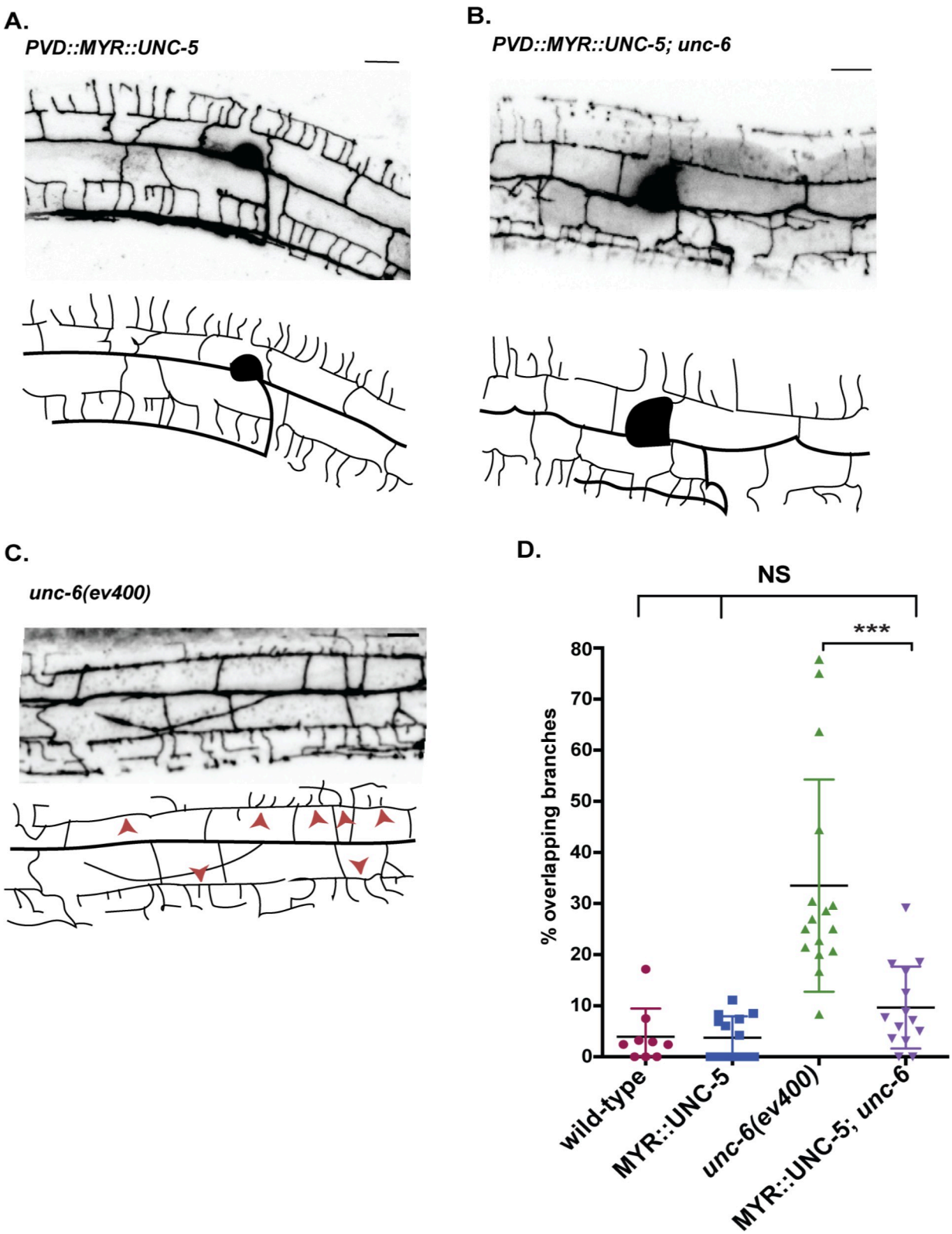

Fig 2. Constitutively active UNC-5 rescues self-avoidance in an *unc-6* mutant. (A-C) Representative images (top) and tracings (bottom) of PVD dendritic architecture in late L4 stage larvae for (A) PVD::MYR:UNC-5, (B) PVD::MYR::UNC-5; *unc-6(ev400)* and (C) *unc-6(ev400)* (See also Fig 8C). (D) Self-avoidance defects (percentage of overlapping 3˚ branches) are rare (< 5%) in wild type and PVD::MYR::UNC-5. The Unc-

6 self-avoidance defect is prevented by PVD expression of MYR::UNC-5. Error bars denote mean and M. ***p<0.0001. n ≥ 15. from ANOVA with Tukey's posthoc test. Scored in a PVD::mCherry background.

https://doi.org/10.1371/journal.pgen.1008228.g002

Mutations that disable actin-polymerizing proteins disrupt dendrite self-avoidance

Genetic tests of additional regulators of actin polymerization also revealed PVD self-avoidance phenotypes. Lamellipodin (Lpd) interacts with ENA/VASP at the tips of filopodia and lamellopodia to extend actin filaments [12,19]. Mutants of *mig-10*/Lpd display robust PVD self-avoidance defects (Fig 3B and 3E). Similarly, self-avoidance is disrupted by a mutation that eliminates the Rac GEF activity of UNC-73/Trio, a potent regulator of actin dynamics [15]. The predicted downstream function of UNC-73/Trio in the UNC-5 signaling pathway [27] is confirmed by our finding that the self-avoidance defects of *unc-73/Trio*, like *unc-34/Ena/VASP* mutants, are fully epistatic to the delayed outgrowth phenotype of constitutively active PVD::MYR::UNC-5 (Fig 3C). We note that both *mig-10*/Lpd and *unc-73*/Trio mutants also show other defects in PVD morphology (e.g., displaced 1˚ dendrite, fewer 2˚ branches) (S2A–S2C Fig) closely resembling those of *unc-34*/Ena/VASP mutants which our results suggest are due to a non-cell autonomous function for UNC-34 (S2A–S2C Fig).

To test for potential roles for branched actin polymerization, we examined a null allele of *wsp-1/WASP* (Wiskott-Aldrich Syndrome protein) and observed defective PVD self-avoidance. If *wsp-1*/WASP functions in a common pathway with *unc-6*, then the self-avoidance defect of the double mutant, *wsp-1; unc-6*, should be no more severe than that of either *wsp-1* or *unc-6* single mutants. We confirmed this prediction by scoring PVD self-avoidance in *wsp-1; unc-6* mutant animals (Fig 3D). An independent study confirmed the role of *wsp-1* in PVD self-avoidance. This work also reported, however, that *wsp-1* does not enhance the self-avoidance defect of a parallel-acting pathway involving MIG-14/Wntless and thus concluded that *wsp-1* functions downstream of MIG-14/Wntless [39]. Additional experiments are needed to resolve the question of whether WSP-1/WASP functions exclusively in the UNC-6/Netrin vs MIG-14/Wntless self-avoidance pathways.

Because WASP is known to activate the Arp2/3 complex [14,40], we also performed RNAi knock down of the conserved Arp2/3 component ARX-5/p21 and detected significant PVD self-avoidance defects (Fig 3E). The canonical roles of WASP and the Arp2/3 complex suggest that self-avoidance depends on the formation of branched F-actin networks. Recent studies have shown that actin and actin regulators like TIAM-1/GEF and components of the Wave Regulator Complex (WRC) are required for PVD dendrite outgrowth [26,27] (S2D Fig). Here our genetic results point to the paradoxical idea that elongation and branching of F-actin filaments are also necessary for dendrite retraction and that this mechanism is activated by UNC-6/Netrin in the self-avoidance response.

The actin cytoskeleton is highly dynamic in growing and retracting PVD dendrites

To test the idea that the actin cytoskeleton is differentially modulated for both outgrowth and retraction we expressed LifeAct::GFP in PVD neurons to monitor actin dynamics during dendrite morphogenesis. Although LifeAct::GFP binds both filamentous actin (F-actin) and monomeric G-actin with high affinity, bright LifeAct::GFP-labeled foci typically correspond to F-actin-containing structures [41]. We observed that the LifeAct::GFP signal was consistently brightest nearest the tips of growing dendrites in comparison to internal dendritic regions (Fig 5B and 5C) as also reported in other studies [26,27,40]. Time-lapse imaging of PVD::LifeAct::

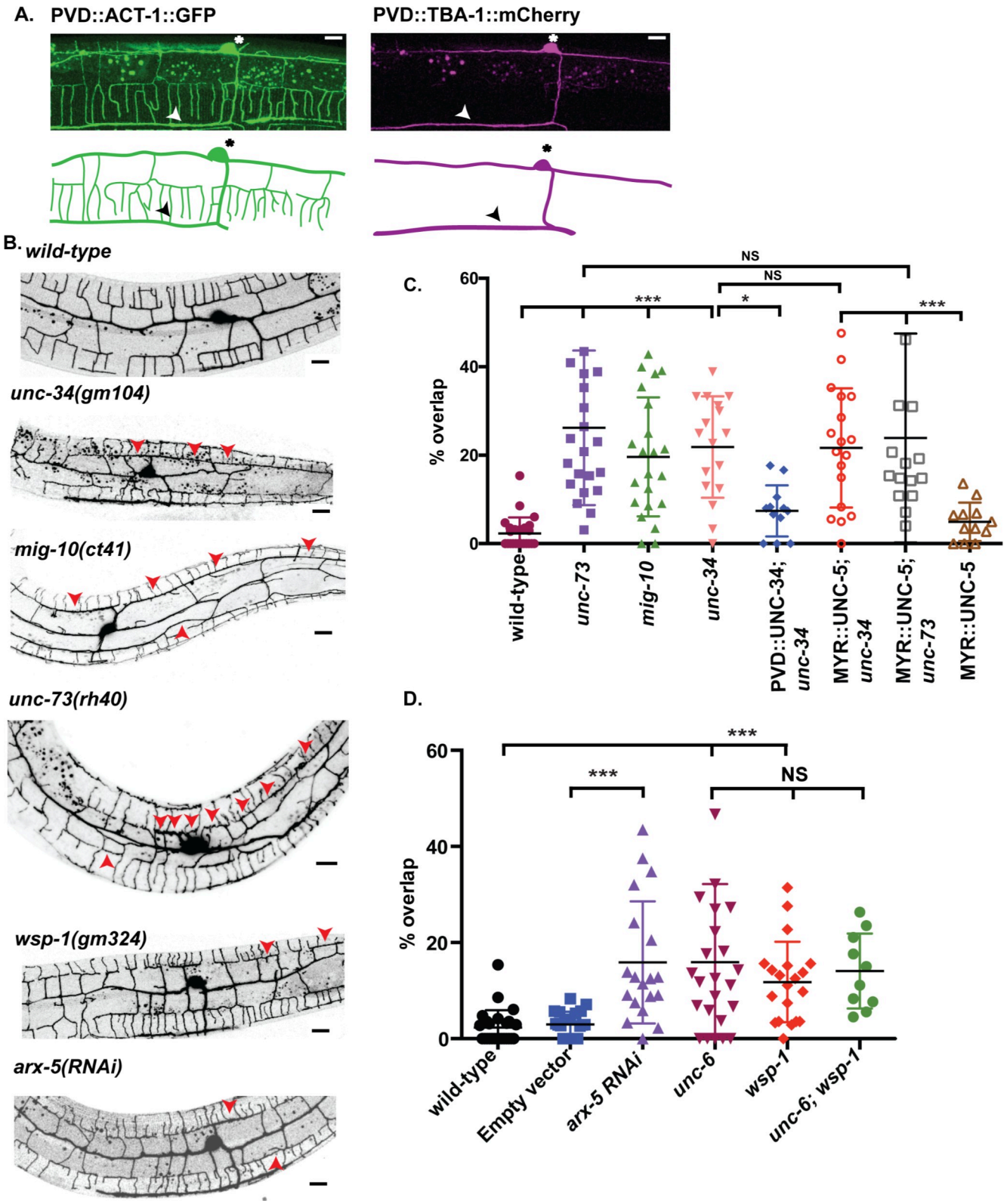

Fig 3. Mutations in genes that promote actin polymerization disrupt PVD dendrite self-avoidance. (A) Representative images (top) and schematics (bottom) of the actin cytoskeleton (green) labeled with PVD::ACT-1::GFP (A) and microtubules (magenta) marked with *pdes-2*::TBA-1::mCherry. PVD cell bodies (asterisks) and axons (arrowheads) are noted. (B) Representative images of PVD::GFP for wild type, for *unc-34*, *mig-10*, *unc-73*, *wsp-1* mutants and

for *arx-5RNAi*. Asterisks denote PVD cell bodies and arrowheads point to overlaps between adjacent PVD 3˚ dendrites. (C-D) Self-avoidance defects are plotted in a PVD::GFP background (mean and SEM) as the percentage of overlapping 3˚ dendrites for each genotype. ***p<0.001, *p<0.05, ANOVA with Tukey's posthoc test, n ≥ 15 animals for all backgrounds. (C) Self-avoidance defects for *unc-73/Trio*, *mig-10/Lmpd* and *unc-34/Ena/VASP* mutants. Self-avoidance defects of *unc-34/Ena/VASP* mutants are rescued by PVD expression of UNC-34 (PVD::mCherry::UNC-34). Constitutively active UNC-5 (PVD::MYR::UNC-5) fails to rescue the self-avoidance defects of an *unc-34* mutant. (D) PVD self-avoidance defects for *arx-5RNAi* compared to Empty Vector RNAi controls., ***p<0.001 and self-avoidance defect of *unc-6*, *wsp-1* and *unc-6; wsp-1* mutants compared to wildtype, NS = Not Significant, ANOVA with Tukey's posthoc test, n ≥ 15 animals. Scale bar is 10 μm.

https://doi.org/10.1371/journal.pgen.1008228.g003

GFP by spinning disk confocal microscopy during the late L3/early L4 stage detected striking, dynamic fluctuations in the LifeAct::GFP signal (S3 Movie). We quantified this effect by comparing time-dependent changes in LifeAct::GFP fluorescence versus that of a PVD::mCherry cytosolic marker. The relatively constant intensity of PVD::mCherry signal in these experiments favors the idea that the observed changes in LifeAct::GFP fluorescence could be due to actin dynamics in growing dendrites (Fig 5A, 5D and 5E).

Because genetic knockdown of actin polymerizing proteins (UNC-34/Ena/VASP, MIG-10/Lpd, UNC-73/Trio, WSP-1/WASP, ARX-5/P21) (Fig 3) disrupts self-avoidance and thus suggests that F-actin is required, we monitored the LifeACT::GFP signal at the tips of 3˚ dendrites during the self-avoidance response (S4 Fig) (S3 Movie). The cytoplasmic mCherry marker was used to detect contact events as instances in which the measured gap between left and right 3˚ dendrites approached zero. Although time-lapse imaging detected dynamic fluctuations in LifeAct::GFP fluorescence both before and after contact, we did not observe a quantitative increase in the LifeACT::GFP signal with retraction (S4 and S5 Figs). Notably, for these experiments, we used the marker strains (i.e., PVD::LifeAct::GFP and PVD::mcherry), imaging strategy (i.e., 40 X objective, 35 s sampling interval) and method of quantitative analysis described in an earlier publication that reported increased LifeAct::GFP fluorescence after contact (N = 14, p = 0.54, two-way ANOVA with Bonferroni correction[39] (S4A–S4C Fig). In an additional approach, we used a higher resolution objective (100X) and longer sampling interval (1–1.3 min) and also did not detect elevated LifeAct::GFP fluorescence during retraction (N = 8, p = 0.74, two-way ANOVA with Bonferroni correction) (S4D Fig and S5 Fig). The simplest explanation of our results is that actin polymerization drives both outgrowth and retraction which are tightly coupled over time at dendrite tips and thus difficult to resolve as separate events.

NMY-1/Non-muscle myosin II drives dendrite retraction in the self-avoidance mechanism

Our imaging results indicate that F-actin is the dominant cytoskeletal structure in growing PVD dendrites. In considering a mechanism to account for dendrite shortening in the self-avoidance response, we hypothesized that a newly synthesized actin cytoskeleton could mediate dendrite shortening by providing a substrate for non-muscle myosin II to drive contraction. To test this idea, we examined loss-of-function alleles that disable the *C. elegans* non-muscle myosins, NMY-1 and NMY-2. This experiment determined that mutations in *nmy-1* but not *nmy*-2 [42] show PVD self-avoidance defects (Fig 6A–6D). This effect is cell autonomous for *nmy-1* because PVD-specific RNAi of *nmy-1* also results in overlapping 3˚ dendrites and PVD-specific expression of GFP-tagged NMY-1 is sufficient to rescue the *nmy-1* self-avoidance defect (Fig 6B–6D). We conclude that a specific non-muscle myosin, NMY-1, promotes dendrite retraction in the self-avoidance mechanism and could act by driving the translocation of F-actin bundles at the tips of 3˚ dendrites.

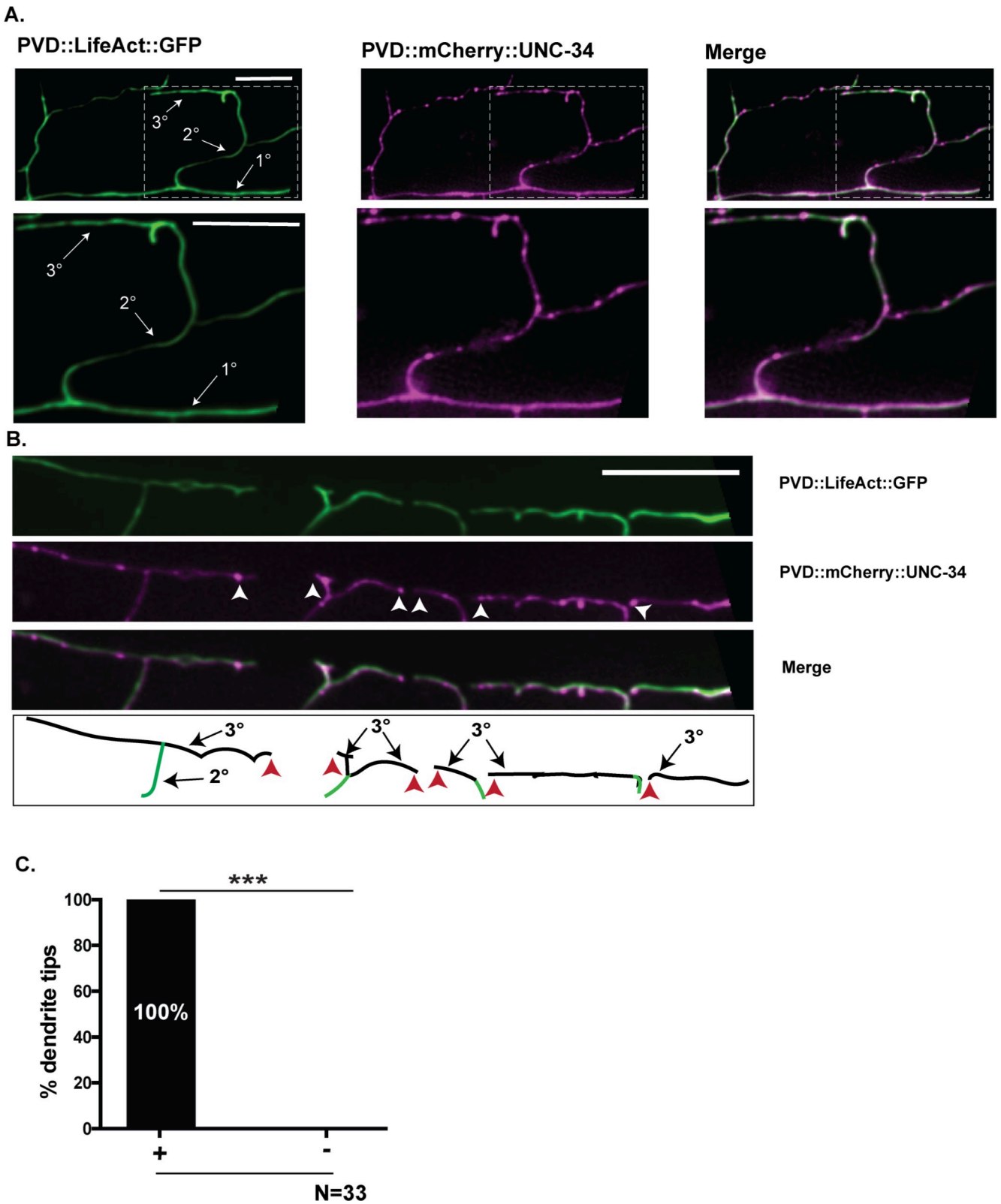

Fig 4. Localization and trafficking of PVD::UNC-34::mCherry puncta in PVD. (A-B) iSIM images (see Methods) of PVD neurons (late L3 larvae) labeled with PVD::LifeAct::GFP (green) and PVD::mCherry::UNC-34 (magenta). Merge shown at top right. Insets depict punctate mCherry::UNC-34 in 1˚, 2˚ and 3˚ PVD dendrites. (B) Note mCherry::UNC-34 puncta at tips (white arrowheads) of 3˚ dendrites. Scale bars are 5 μm. (C) Frequency (100%) at which tips of

3˚ dendrites show mCherry::UNC-34 puncta, ***p<0.001, Fischer's exact test, N = 33 dendrite tips in 9 animals. Both iSIM and Airyscan images (S3 Fig, S1 Methods) were used in this analysis.

https://doi.org/10.1371/journal.pgen.1008228.g004

Phosphomimetic activation of MLC-4 shortens PVD 3˚ dendrites

Non-muscle myosin II motor proteins are composed of myosin heavy chain (MHC) and light chains, the essential light chain (ELC) and regulatory light chain (RLC) [43,44]. Myosin motor activity is triggered by RLC phosphorylation that induces a conformational change to allow assembly of the myosin complex into active bipolar filaments (Fig 7A) [45]. Having shown that NMY-1/non-muscle myosin is required for self-avoidance, we next performed an additional experiment to ask if constitutive non-muscle myosin activity is sufficient to induce dendrite retraction. For this test, we expressed a phosphomimetic mutant of MLC-4, the *C. elegans* RLC homolog. MLC-4/myosin regulatory light chain contains serine/S and threonine/T phosphorylation sites in a highly-conserved domain. Both S and T residues were mutated to Aspartate/D and the resultant phosphomimetic construct MLC-4DD was fused to GFP for transgenic expression in PVD (Fig 7B and 7C) [46]. PVD neurons that expressed MLC-4DD showed significantly shorter 3˚ dendrites at the L3 stage in comparison to wild type as well as a concurrent increase in the width of gaps between 3˚ dendrites from adjacent menorahs (Fig 7D–7G). These phenotypic traits are consistent with the idea that normal dendrite outgrowth is slowed by constitutive activation of non-muscle myosin by MLC-4ADD. By the L4 stage, PVD architecture in the MLC-4DD strain resembles that of the wild type with normal appearing menorah morphology and spacing (Fig 8A and 8B). Similar results were observed for PVD neurons that express constitutively active MYR::UNC-5 which we have proposed functions downstream of UNC-6/Netrin to trigger the self-avoidance response (Fig 2D). Our finding that MLC-4DD rescues the self-avoidance defect of *unc-6* mutants suggests that NMY-1/non-muscle myosin II also functions downstream of *unc-6* for dendrite retraction (Fig 8D). Alternatively, rescue of the Unc-6 phenotype by MLC-4DD could be indicative of NMY-1/non-muscle myosin II acting in parallel to *unc-6*.

Antagonistic pathways regulate dendrite outgrowth vs self-avoidance

Our time lapse imaging studies detected dynamic actin polymerization in growing PVD dendrites (S3 Movie). This observation and the recent finding that PVD dendrites are truncated and misdirected by mutations that disable either a the actin structural gene, *act-4*, or specific components (WRC and TIAM/GEF) that promote actin polymerization, suggest that dendritic outgrowth depends on actin assembly [26,27] (S2D Fig). Actin assembly is also likely required for dendrite retraction given results showing that genetic knockdown of a separate set of actin-binding proteins (i.e., UNC-34/Ena/VASP, MIG-10/Lpd, UNC-73/Trio, WSP-1/WASP, ARX-5/p21) (**Fig 3**), blocks PVD self-avoidance but not dendrite outgrowth [39]. A shared role for actin polymerization in both outgrowth and retraction argues that the net length of PVD dendrites must depend on an intrinsic mechanism that regulates actin assembly to balance these competing effects.

Our results suggest that UNC-6/Netrin signaling promotes dendrite retraction in a mechanism involving F-actin assembly. PVD dendritic outgrowth is driven by a separate pathway in which DMA-1, a membrane protein expressed in PVD, interacts with a multicomponent receptor anchored in the adjacent epidermis [13,45–49]. Dendritic growth depends on binding of DMA-1 and the claudin-like protein, HPO-30, to specific regulators of actin assembly (i.e., WAVE regulatory complex, TIAM-1/GEF) in the PVD cytoplasm [26,27,50]. These interactions may be modulated by the Furin KPC-1 which antagonizes DMA-1 surface expression in

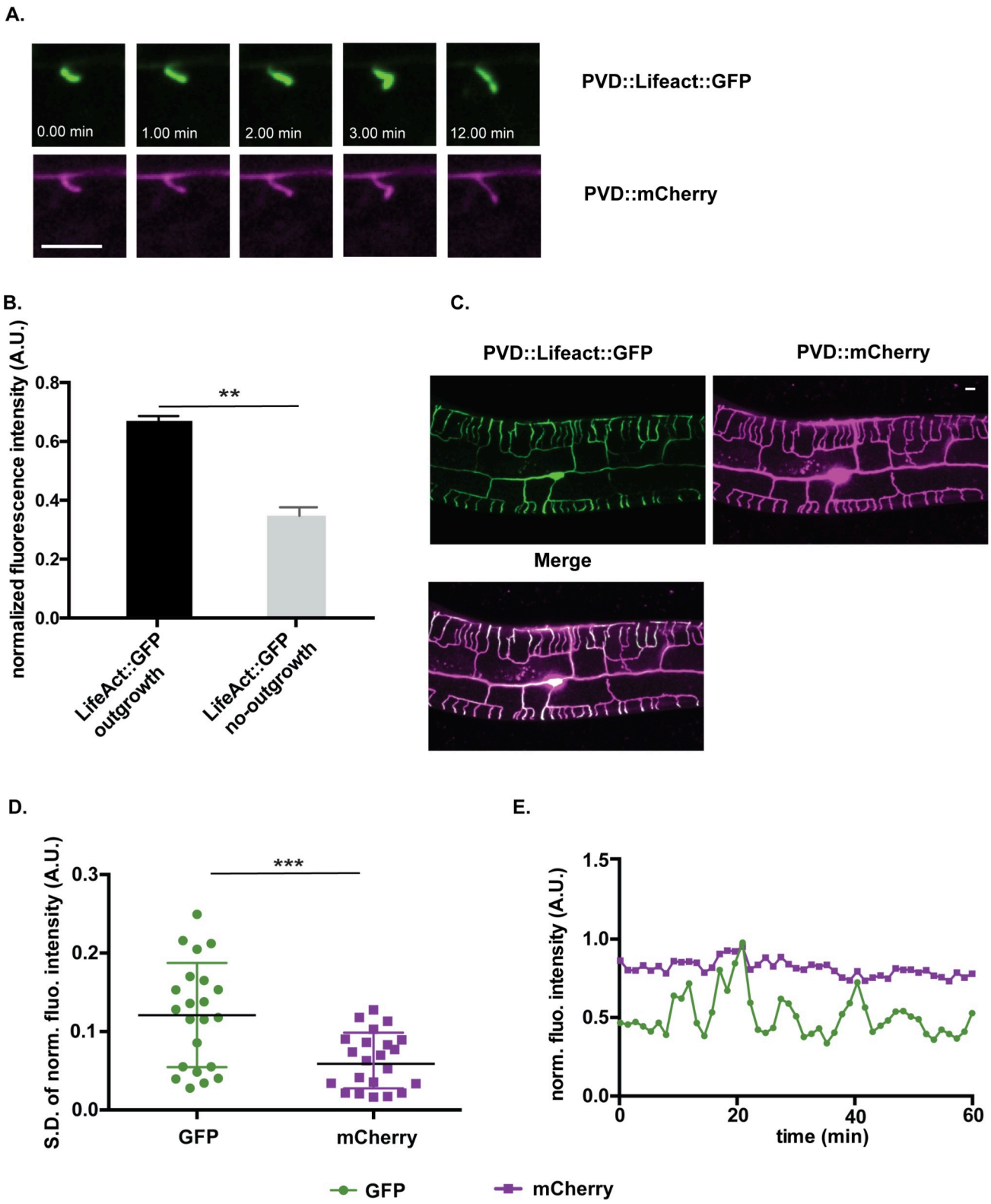

Fig 5. The actin cytoskeleton is highly dynamic in PVD dendrites. (A) Time-lapse images of PVD::LifeAct::GFP and cytosolic PVD::mCherry labeled 2° dendrite during outgrowth (late L3 larvae). (B) Fluorescent intensity was measured from regions of PVD dendrites undergoing outgrowth vs no-outgrowth (see Materials and Methods). ***p<0.001, N = 118 measurements from 6 dendrites. (C) Representative image showing enriched LifeAct::GFP signal in distal, growing PVD dendrites labeled with PVD::mCherry. (D) Rapid changes in the normalized fluorescence intensity of PVD::LifeAct::GFP

versus the PVD::mCherry cytoplasmic marker were quantified as the standard deviation of the normalized fluorescent intensity measured at the tips of growing dendrites. (See S3 Movie and Methods) ***p = 0.003, N = 22. (Unpaired t-test) (E) Normalized fluorescence intensity measurements of PVD::LifeAct::GFP (green) vs cytoplasmic PVD::mCherry (red) at the tip of a growing late L3 stage PVD 3˚dendrite from a representative time lapse movie.

https://doi.org/10.1371/journal.pgen.1008228.g005

PVD [47–49]. *kpc-1* activity is proposed to temporally weaken adhesion with the epidermis to facilitate changes in trajectory at specific stages in dendritic outgrowth [49,50]. For example, the tips of 3˚ branches typically execute a right-angle turn after the self-avoidance response to produce a 4˚ dendrite [11]. This morphological transition largely fails in *kpc-1* mutants in which 3˚ dendrites elongate abnormally and show severe self-avoidance defects due to over-

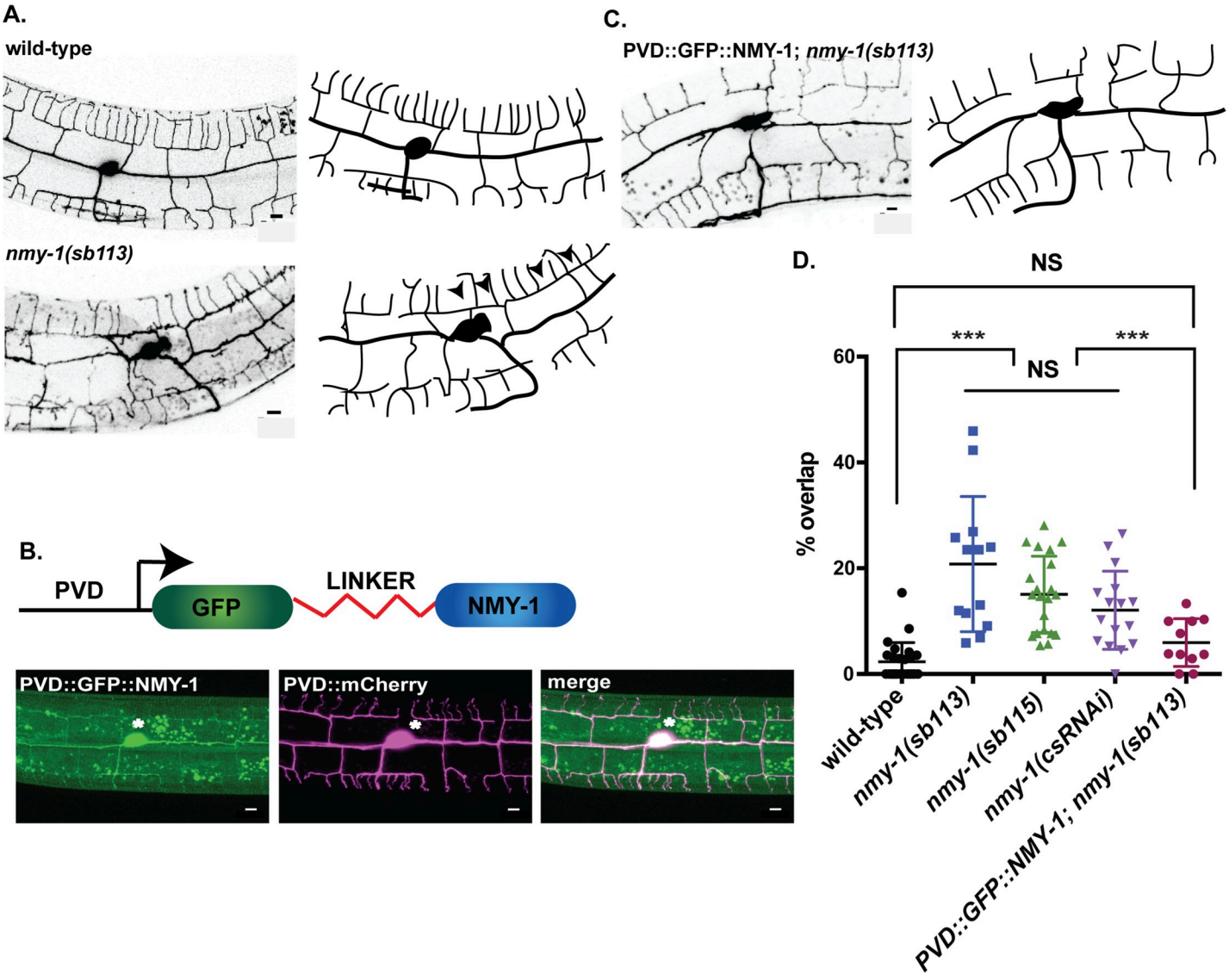

Fig 6. NMY-1/non-muscle myosin II mediates dendrite self-avoidance. (A) Representative images (left) and tracings (right) of wild type and *nmy-1(sb113)* labeled with PVD::GFP. Arrowheads mark overlapping 3˚ dendrites. The PDE neuron (asterisk) is adjacent to the PVD cell-body. (B) NMY-1 fused to GFP via a linker peptide (PVD::GFP::NMY-1) (top) expressed in PVD with PVD::mCherry (bottom) rescues self-avoidance defects (C) of *nmy-1(sb113)*. Scale bars are 50μm. (D) Quantification of self-avoidance defects in wild type and *nmy-1*. The percentage of overlapping 3˚ branches is elevated in *nmy-1* mutants and with *nmy-1* cell-specific RNAi (csRNAi) vs wild type. PVD expression of GFP-labeled NMY-1 (PVD::GFP::NMY-1) rescues the *nmy-1(sb113)* self-avoidance defect. Scatter plots with mean and SEM, ***p<0.01, One way ANOVA with Tukey's posthoc test. N = 15–20 animals per genotype. All defects were quantified in a PVD::GFP background. Scale bar is 5 μm.

https://doi.org/10.1371/journal.pgen.1008228.g006

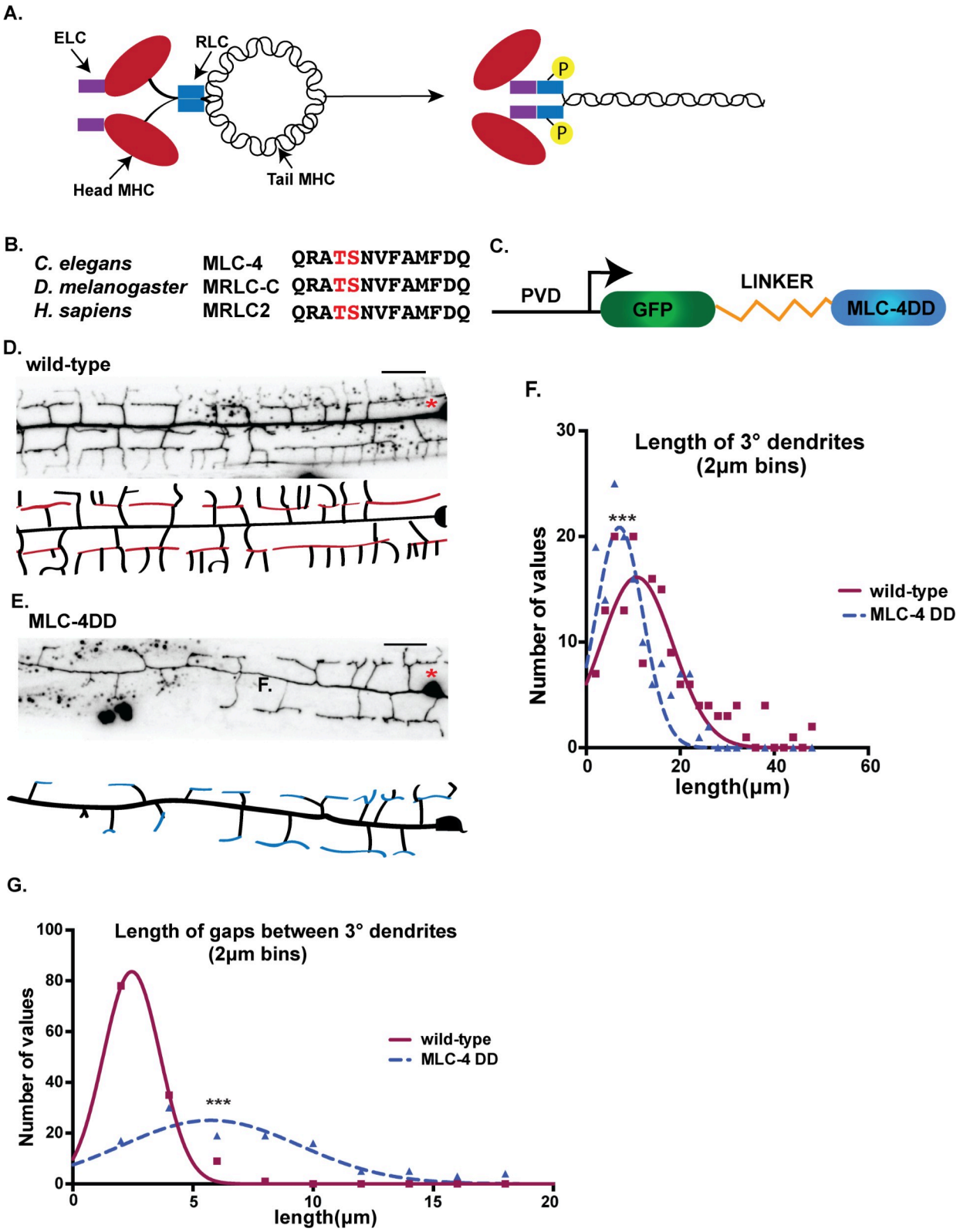

Fig 7. Phosphomimetic activation of myosin regulatory light chain, MLC-4, retards outgrowth of 3˚ PVD dendrites. (A) Phosphorylation of Regulatory Light Chain (RLC) induces a conformational change that activates the myosin protein complex composed of myosin heavy chain (MHC), essential light chain (ELC) and RLC. (B) Threonine and serine phosphorylation sites (red) in conserved regions of *C. elegans*, *Drosophila*

and human myosin RLCs. (C) Phosphomimetic construct, PVD::GFP::MLC-4-DD, fused to GFP with a linker peptide for expression with PVD promoter. (D-E) Representative images (top) and schematics (bottom) of PVD morphology anterior to cell body (asterisk) denoting 3˚ dendrites for (D) wild type (red) and (E) MLC-4DD (blue) (L3 stage larvae). Wild-type image also used in Fig 2A. Scale bars are 10 μm. 3˚ dendrite length (F) is shorter and gaps between 3˚ dendrites (G) is wider for MLC-4DD versus wild type at the L3 stage. Gaussian fit was plotted with bin center values (μm) on the X-axis and the number of values that fall under each bin center on the Y axis, ***$p<0.001$, Kolmogorov-Smirnov test for cumulative distributions of PVD 3˚ dendrite lengths and length of gaps in MLC-4DD (n = 141, 6 animals) versus wild type (n = 156, 8 animals). Scale bar is 10 μm.

https://doi.org/10.1371/journal.pgen.1008228.g007

expression of DMA-1 [49,50]. Thus, we considered the idea that self-avoidance is achieved by the combined effects of *kpc-1*-dependent downregulation of DMA-1 and a separate mechanism that antagonizes outgrowth and requires UNC-6/Netrin. We performed a series of genetic experiments to test this model.

The hypomorphic loss-of-function allele, *kpc-1(xr58)*, results in over-expression of DMA-1 and a consequent, robust self-avoidance defect with ~42% of sister 3˚ branches overlapping one another (Fig 9A and 9D) [48,49]. This defect is not observed, however, in *kpc-1*/+ heterozygotes (Fig 9D). Similarly, self-avoidance in *unc-6*/+ heterozygous animals is indistinguishable from wild type (Fig 9D). Thus, a 2-fold reduction in gene dosage for either *kpc-1* or *unc-6* does not perturb self-avoidance. We reasoned, however, that if expression of UNC-6/Netrin and KPC-1 were simultaneously reduced by half, then self-avoidance should be at least partially disabled since both *unc-6* and *kpc-1* normally function to antagonize dendrite outgrowth. To test this prediction, we constructed double heterozygous mutants of *kpc-1* and *unc-6* (e.g., *kpc-1*/+; *unc-6*/+) and quantified the self-avoidance phenotype. This experiment revealed that ~30% of adjacent sister 3˚ dendrites fail to self-avoid in *kpc-1*/+; *unc-6*/+ animals which is significantly greater than that of either *kpc-1*/+ or *unc-6*/+ single mutants (Fig 9B and 9D). This genetic "enhancer" effect is consistent with the idea that both KPC-1 and UNC-6 function to limit growth of 3˚ dendrites. If this effect is due to elevated levels of DMA-1 arising from reduced KPC-1 activity in the *kpc-1*/+; *unc-6*/+ background, then a concomitant diminution of DMA-1 activity should restore normal self-avoidance. We tested this idea by constructing the triple heterozygote, *kpc-1* +/+ *dma-1; unc-6*/+, and detected robust suppression of the self-avoidance defect observed in *kpc-1*/+; *unc-6*/+ animals (Fig 9C and 9D). Thus, these results suggest that DMA-1-mediated adhesion to the epidermis antagonizes UNC-6/Netrin-dependent dendrite retraction and that the relative strengths of these opposing pathways must be finely tuned to achieve the self-avoidance effect (Fig 9E). The key role of actin polymerization in both UNC-6/Netrin-mediated retraction and DMA-1-dependent outgrowth argues that this balancing mechanism likely regulates both modes of actin assembly.

Discussion

Dendrites arising from the same neuron typically do not overlap. This phenomenon of dendrite self-avoidance is universally observed and derives from an active mechanism in which contact between sister dendrites triggers mutual retraction [4,48]. As might be predicted for an event that depends on physical proximity, cell-surface associated proteins have been shown to mediate dendrite self-avoidance [39,51]. These include Dscam and protocadherins which are expressed in multiple alternative forms to distinguish self from non-self among contacting dendrites [5–7]. Self-avoidance for certain neurons can also depend on the interaction of diffusible cues with their cognate receptors [8,51]. For example, we have shown that the axon guidance signal, UNC-6/Netrin, and its receptors, UNC-5 and UNC-40/DCC, function together to mediate self-avoidance for PVD sensory neurons in *C. elegans*. We have proposed that UNC-40/DCC captures UNC-6/Netrin on the membrane surface to facilitate repulsion through physical interaction with UNC-5 on PVD dendrites [9] (S1D Fig). Little is known,

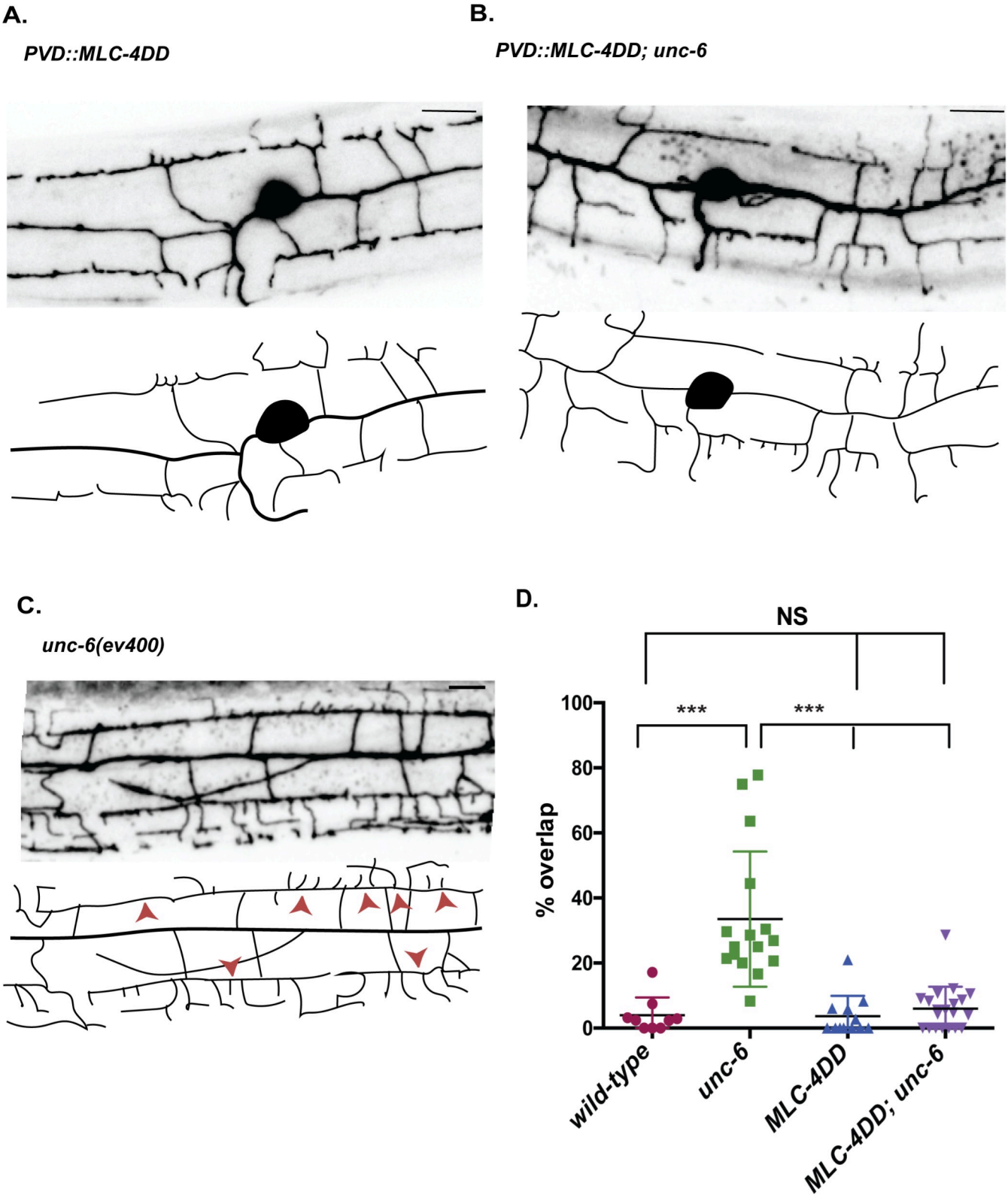

Fig 8. Phosphomimetic activation of myosin regulatory light chain, MLC-4, rescues the *unc-6* dendritic self-avoidance defect. (A-C) Representative images and tracings of PVD dendritic architecture in late L4 stage larvae for (A) PVD::MLC-4DD, (B) PVD::MLC-4DD; *unc-6(ev400)* and (C) *unc-6(ev400)*. (D) PVD expression of MLC-4DD rescues the *unc-6* mutant self-avoidance defect in L4 animals, $^{***}p<0.0001$, one-way ANOVA with Tukey's posthoc test. Mean and SEM are shown. n ≥ 9 animals per genotype. Quantified with PVD::mCherry. Scale bar is 10 μm. wild-type and *unc-6(ev400)* results from Fig 2D. The image for *unc-6(ev400)* is also shown in Fig 2C.

https://doi.org/10.1371/journal.pgen.1008228.g008

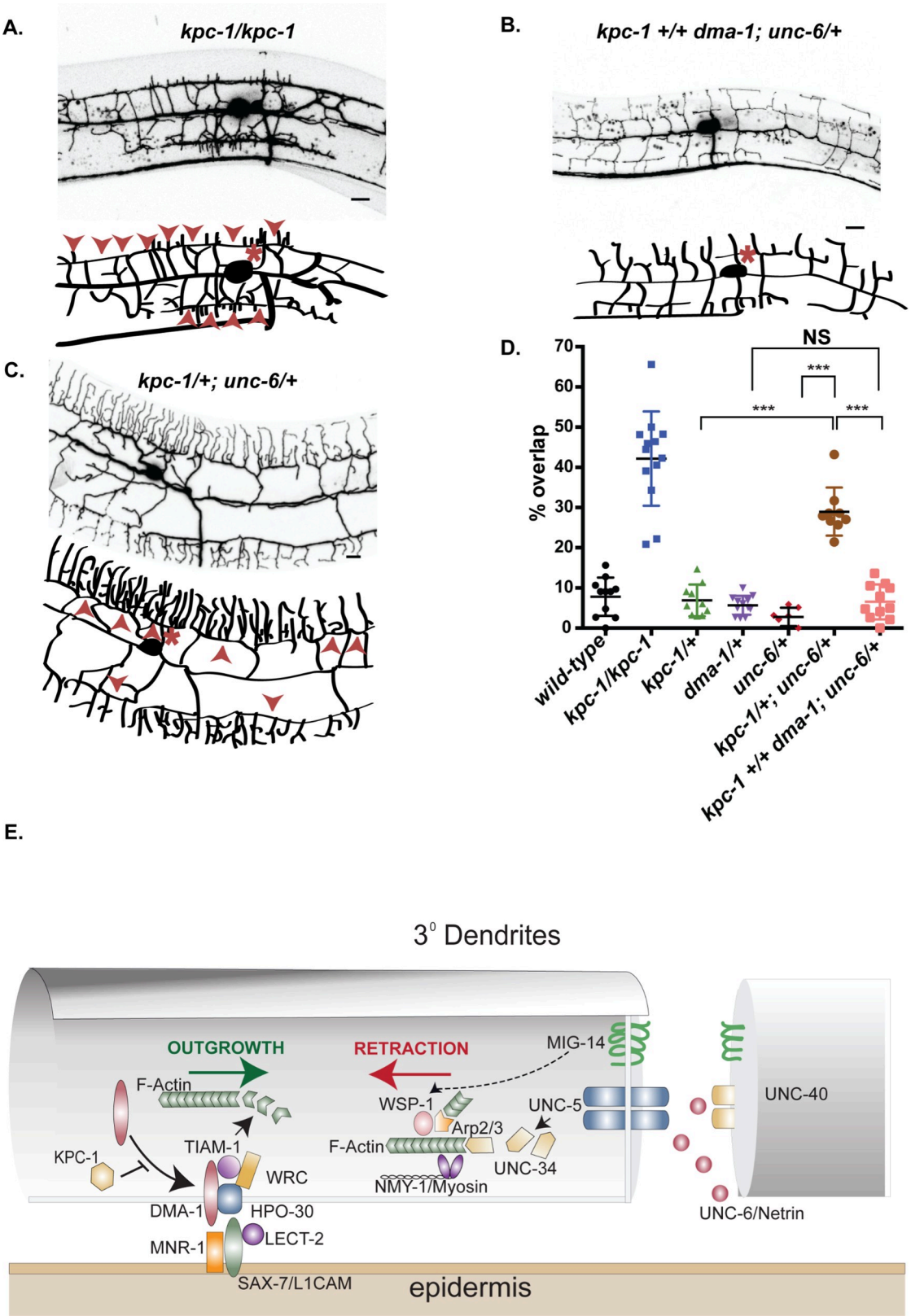

Fig 9. Opposing pathways regulate dendrite outgrowth versus retraction. Representative images and schematics of PVD in (A) *kpc-1/kpc-1*, (B) *kpc-1/+; unc-6/+* and (C) *kpc-1 +/+ dma-1; unc-6/+*. PVD soma (asterisks) and overlapping 3° dendrites

(arrowheads) are noted. (D) Quantification of self-avoidance defects for each genotype. Note that all mutant alleles are recessive but that *kpc-1/+; unc-6/+* double heterozygotes show a strong self-avoidance defect that is suppressed in *kpc-1 +/+ dma-1; unc-6/+* triple heterozygotes. ***p<0.0001, one way ANOVA with Tukey's posthoc test. Mean and SEM are indicated. *** p <0.0001, N ≥7 animals per genotype. PVD is labeled with *ser2prom3*::GFP for all images. Scale bar is 10 μm. Mutant alleles were: *kpc-1(xr58)*, *unc-6 (ev400)* and *dma-1(wy686)*. (E) Model of opposing pathways that promote actin polymerization to define dendrite length. KPC-1 antagonizes surface expression of DMA-1 that interacts with an epidermal receptor composed of SAX-7/CAM, MNR-1 and LECT-2 and functions with HPO-30 to activate TIAM-1/GEF and the Wave Regulatory Complex (WRC) for actin polymerization and dendrite outgrowth. UNC-6/Netrin is captured by UNC-40/DCC for interaction with UNC-5 to activate UNC-34/Ena/VASP which functions with WSP-1/WASP and the Arp2/3 complex to drive F-actin assembly for NMY-1/myosin-dependent dendrite retraction in the self-avoidance response. (UNC-73/Trio and MIG-10/Lamellipodin are not shown to simplify the diagram, see Results). Homotypic interaction of MIG-14/Wntless in contacting 3^{O} dendrites also drives retraction possibly through WSP-1.

https://doi.org/10.1371/journal.pgen.1008228.g009

however of the downstream effectors of dendrite retraction in the self-avoidance response. Here we report new results that are consistent with a model in which UNC-6/Netrin promotes actin-polymerization to propel dendrite retraction. Our finding that non-muscle myosin is also involved resolves the paradoxical idea that UNC-6/Netrin-dependent actin polymerization shortens rather than lengthens PVD 3˚ dendrites. We propose that non-muscle myosin engages the nascent F-actin cytoskeleton at the tips of PVD dendrites to drive retraction.

Regulators of actin polymerization are required for dendrite self-avoidance

The proposed role for actin polymerization in the self-avoidance response derives from our finding that multiple regulators of F-actin assembly are necessary for efficient dendrite retraction. For example, a mutation that disables UNC-34, the *C. elegans* homolog of Ena/VASP, disrupts PVD self-avoidance. Ena/VASP promotes actin polymerization by preventing capping proteins from blocking the addition of actin monomers to the plus-end of elongating actin filaments. In axonal growth cones, Ena/VASP localizes to the tips of actin bundles in growing filopodia [12,38]. We observed punctate Ena/VASP localization at the tips of PVD dendrites (Fig 4 and S3 Fig). Our results showing that an *unc-34* mutant suppresses the retarded dendrite outgrowth phenotype arising from the constitutively active MYR::UNC-5 (Fig 3C) argues that *unc-34* functions downstream to mediate UNC-6/Netrin-dependent self-avoidance. Additional genetic evidence indicates that WSP-1/WASP also acts in a common pathway with UNC-6/Netrin (Fig 3D). The established role for WASP of activating the Arp2/3 complex [52] is consistent with our finding that RNAi knockdown of *arx-5/p21*, a conserved Arp2/3 component, partially disables the self-avoidance mechanism (Fig 3D). Dual roles for UNC-34 and WSP-1 in actin polymerization, as suggested here, are also consistent with previous work indicating that Ena/VASP can activate Arp2/3 through direct interaction with WASP proteins [33,53–55]. Thus, taken together, our results suggest that Ena/VASP and WSP-1 coordinate the creation of branched actin networks at the tips of retracting PVD dendrites in the UNC-6/Netrin dependent self-avoidance response (Fig 9E).

A role for Ena/VASP in dendrite retraction, as proposed here, parallels earlier findings of a necessary function for Ena/VASP in growth cone repulsion. For example, axon guidance defects arising from ectopic expression of UNC-5 in *C. elegans* touch neurons requires UNC-34/Ena/VASP [56], a finding consistent with our observation that the dendritic shortening phenotype induced by MYR::UNC-5 is prevented by a loss-of-function mutation in *unc-34*. Ena/VASP is also required for axon repulsion mediated by Slit and its receptor Robo [20,57,58]. Although Ena/VASP function can be readily integrated into models of axonal attraction, the well-established role of Ena/VASP in F-actin assembly has been more difficult to rationalize in mechanisms of axonal repulsion which are presumed to involve actin depolymerization [12,59]. A partial explanation for this paradox is provided by a recent study showing that Slit, acting through Robo, induces transient filopodial outgrowth in migrating axonal

growth cones and that this effect requires Ena/VASP [58]. The functional necessity for filopodial growth in this mechanism is unclear, but the central role of Ena/VASP-induced actin assembly in the overall repulsive response to Slit mirrors our results suggesting that dendrite retraction in PVD neurons requires UNC-34/Ena/VASP and F-actin assembly.

Our studies also detected necessary roles in self-avoidance for two additional components, MIG-10/LPD which has been previously shown to function with UNC-34/Ena/VASP to promote F-actin polymerization and UNC-73/Trio, a Rho/Rac GEF that acts in UNC-6/Netrin pathways to regulate the actin cytoskeleton [15,19,20,27]. Altogether, our genetic analysis identified five known effectors of actin polymerization (UNC-34/Ena/VASP, WSP-1/WASP, Arp2/3 complex, MIG-10/Lpd, UNC-73/Trio) that mediate the self-avoidance response but which are not required for 3˚ branch extension during outgrowth (Fig 3B and 3C, S2A–S2C Fig).

Non-muscle myosin II mediates dendrite retraction in the self-avoidance response

Our genetic analysis detected a cell-autonomous role for NMY-1/non-muscle myosin II in dendrite self-avoidance (Fig 6A–6D). Because our results revealed F-actin at the tips of PVD dendrites (Fig 5), we suggest that NMY-1 mediates retraction by interacting with F-actin to drive a contractile mechanism. For example, NMY-1 could accelerate retrograde flow, a non-muscle myosin-dependent effect that also drives filopodial retraction in growth cones and at the leading edge of migrating cells [60,61]. Alternatively, NMY-1 could shorten PVD dendrites by inducing the reorganization of the nascent actin cytoskeleton into a more compact structure [62]. Phosphorylation of myosin regulatory light chain (RLC) activates non-muscle myosin [45] and we showed that MLC-4DD, a phosphomimetic, and, thus, constitutively active form of the *C. elegans* homolog of RLC, results in delayed outgrowth of PVD 3˚ dendrites (Fig 7A–7G). The retarded dendrite outgrowth resulting from chronic activation of MLC-4 suggests a model in which NMY-1 function is triggered by contact between sister dendrites and subsequent UNC-6/Netrin signaling. A downstream function for non-muscle myosin II in the UNC-6/Netrin pathway is consistent with our finding that the Unc-6 self-avoidance defect is rescued by MLC- 4DD (Fig 8D). Parallel roles for these components in axon guidance are suggested by recent results showing that non-muscle myosin II is required for Slit and Netrin-dependent midline avoidance in the developing vertebrate spinal cord [63]. Similarly, non-muscle myosin II mediates Semaphorin-induced axonal repulsion. The mechanism of Semaphorin action in this case also involves the assembly of actin bundles in the axon shaft presumably to facilitate non-muscle myosin-driven retraction [64–66]. Thus, our findings suggest that key drivers of axonal repulsion including nascent actin assembly and non-muscle myosin may also mediate dendrite retraction in the self-avoidance response.

RLC phosphorylation activates non-muscle myosin II by releasing myosin monomers for assembly into bipolar structures or myosin "stacks" that interact with actin filaments to induce translocation [45,67]. Although our results are consistent with a necessary role for non-muscle myosin in dendrite retraction, the tips of PVD 3˚ dendrites are likely too narrow (~50 nm) [10] to accommodate myosin stacks (~300 nm) [67,68]. We suggest that the actin-branching function of Arp2/3, which we have shown mediates PVD dendrite retraction, could induce transient expansion of the dendritic tip to allow assembly of myosin stacks. In this model, actin-polymerization involving Arp2/3 could effectively limit ectopic NMY-1 activation in the dendritic shaft by restricting the assembly of myosin stacks to the tips of contacting sister dendrites. Alternatively, recent evidence indicates that myosin can also induce contraction in its monomeric or unpolymerized form [69] which should have ready access to the dendrite tip. This idea is consistent with our observation that GFP-tagged NMY-1 is active (e.g., rescues the

self-avoidance defect of *nmy-1*) and did not display the punctate appearance characteristic of myosin stacks (Fenix et al., 2016) but is diffusely localized throughout the PVD cytoplasm (Fig 6B).

Parallel-acting pathways regulate dendrite self-avoidance

Although self-avoidance is perturbed in UNC-6/Netrin pathway mutants, a significant fraction (~70%) (Fig 3D) of PVD 3˚ dendrites show apparently normal self-avoidance behavior [9]. One explanation for this observation is provided by the recent discovery of an independent pathway, mediated by MIG/14/Wntless, that is necessary for self-avoidance in an additional fraction of PVD 3˚ dendrites [39]. Parallel acting pathways also mediate self-avoidance in mammalian Purkinje neurons where slit-robo signaling acts in concert with protocadherins (Gibson et al., 2014; Lefebvre et al., 2012). The likelihood of additional effectors of self-avoidance is also suggested by the incompletely penetrant effects of Dscam mutants in Drosophila sensory neuron self-avoidance (Matthews and Grueber, 2011). Thus, our results in *C. elegans* mirror findings in other organisms which together suggest that multiple mechanisms have evolved to insure dendrite self-avoidance.

The actin cytoskeleton is highly dynamic in growing and retracting PVD dendrites

We used time-lapse imaging with LifeAct::GFP, a live-cell marker for actin [41], to monitor actin PVD dendrites. The LifeAct::GFP signal is typically brighter near the distal ends of growing branches in comparison to interstitial regions (Fig 5B and 5C) and is highly dynamic (S3 Movie). The distal localization and rapidly fluctuating LifeAct::GFP signal in PVD dendrites resembles recently reported "actin blobs" that actively migrate in highly branched Drosophila sensory neurons where they appear to presage points of branch initiation [70]. A strong LifeAct::GFP signal at the tips of emerging PVD dendrites is also consistent with genetic evidence that actin polymerization is required for dendrite outgrowth [24,25]. Although our genetic results (Fig 3) suggest a model of dendrite retraction in which nascent actin polymerization is necessary for the self-avoidance response, our measurements did not detect a quantitative increase in LifeAct::GFP in retracting vs growing 3˚ dendrites as previously reported by others [39]. This result suggests that the overall level of actin polymerization is high during both outgrowth and retraction but may be incorporated into distinct structures, regulated by distinct groups of effectors (see below) that our imaging methods do not resolve.

Antagonistic pathways regulate dendrite outgrowth vs retraction

Dendritic architecture is defined by the combined effects of outgrowth which expands the arbor vs retraction which limits the size of the receptive field. This interaction of positive and negative effects is readily observed in the development of 3˚ PVD dendrites. Initially, 3˚ dendrites emanating from adjacent menorahs grow out along the body axis until contacting one another and then retract to avoid overlap [9,11]. Outgrowth in this case is promoted by a multicomponent receptor-ligand complex that mediates adhesive interactions with the adjacent epidermis [71–74] (Fig 9E). When this pathway is dysregulated by over-expression of the DMA-1 receptor in PVD neurons, for example, 3˚ dendrites continue to adhere to the epidermis and overgrow one another [49,75]. 3˚ branch self-avoidance also fails in mutants that disable UNC-6/Netrin signaling which we have shown promotes dendrite retraction [9]. Thus, these results suggest that the net length and placement of each 3˚ branch depends on the balanced effects of locally acting signals that either extend (e.g., DMA-1) or shorten (e.g., UNC-6/Netrin) the dendrite. We confirmed this idea in genetic experiments that detected strong dose-

sensitive interactions between these opposing pathways. For example, a 50% reduction of UNC-6/Netrin expression in a heterozygous *unc-6*/+ mutant does not perturb self-avoidance. Similarly, a genetic mutant (*kpc-1/+)* that partially elevates DMA-1 also shows normal 3˚ branch outgrowth. The combination of both mutations in the double heterozygote, *unc-6/+; kpc-1*/+, however, produces a strong self-avoidance defect (Fig 9A–9D). Our genetic results identified multiple regulators of actin polymerization (UNC-34/Ena/VASP, WSP-1/WASP, ARX-5/p21, MIG-10/Lamelipodin, UNC-73/Trio) that are required for self-avoidance (Fig 3). We thus propose that UNC-6/Netrin promotes actin polymerization to effect dendrite retraction and that non-muscle myosin II interacts with a nascent actin cytoskeleton to translocate each 3˚ dendrite away from its neighbor. F-actin is also abundant and highly dynamic in growing PVD dendrites. Notably, a distinct set of F-actin promoting factors (WRC, TIAM/GEF) interacts with the DMA-1 receptor complex to drive PVD dendritic growth (Fig 9E) [26,27]. Additional genetic evidence suggests that the WRC could also function in self-avoidance [39]. Thus, the challenge for future studies is to elucidate the cell biological machinery through which opposing pathways manipulate the actin cytoskeleton to effect either dendrite growth or retraction.

Materials and methods

Strains and genetics

All the strains used were maintained at 20˚C and cultured as previously described (Brenner, 1974). We used the N2 Bristol strain as wild-type.

Additional strains used in this study: NC1404 [*wdIs52* (*pF49H12.4*::GFP)], NW434 [*unc-6 (ev400)X*;*wdIs52(pF49H12.4*::*GFP)*], TV17,200 [*kpc-1(xr58); wyIs592(pser2prom3*::*GFP)*] [49], TV9656 [*dma-1(wy686); unc-119(ed3)III; wyEx3355(pser2prom3*::*GFP+odr-1*::*RFP)*], CX1248 [*KyEx3482*(*pdes-2*::*TBA-1*::*mCherry+coel*::*RFP*)] [28], CLP928 [*twnEx382(Pser2.3*::*LifeAct*:: *EGFP*, *Pser2.3*::*mCherry*, *Pgcy-8*::*gfp)*] [39].

Additional strains generated for this study: NC2580 *unc-34(gm104)V*; *wdIs52*, NG324 [*wsp-1(gm324)*; *wdIs52*], *+/szT1 lon-2(e678) I;* HR1184 [*nmy-1(sb115) dpy-8(e130)/szT1 X*], NC2726 [*nmy-1(sb113)*;*wdIs52*], *unc-73(rh40)*]; *wdIs52*.

NC3284 [*wdEx1011* (*pF49H12.4*::myrUNC-5::GFP)], was produced by microinjection of plasmids pLSR18 (*pF49H12.4*::myrUNC-5::GFP), *pmyo-2*::mCherry and pCJS04 (*pF49H12.4*:: mCherry).

NC3048 [*wdIs98* (*pF49H12.4*::ACT-1::GFP)] was produced by microinjection of plasmids pLSR03 (*pF49H12.4*::ACT-1::GFP) and *pceh-22*::GFP and integrated as previously described (Miller and Niemeyer, 1995).

NC3085 [*wdEx967* (*pF49H12.4*::mCherry::UNC-34)] was obtained by microinjection of plasmids pCJS78(*pF49H12.4*::mCherry::UNC-34) and *pmyo-2*::mCherry.

NC3090 [*wdEx972* (*pF49H12.4*::LifeAct::GFP)] was acquired by microinjecting plasmids pLSR06 (*pF49H12.4*::LifeAct::GFP) and *pmyo-2*::mCherry.

NC3029 [(*pF49H12.4*::*nmy-1(+)* + *pF49H12.4*::*nmy-1(-)*)] was obtained by microinjection of pLSR09 (*pF49H12.4*::*nmy-1(+)*), pLSR10 (*pF49H12.4*::*nmy-1(-)*), pmyo-2::mCherry and pCJS04 (*pF49H12.4*::mCherry)

NC3087 [*wdEx969* (*pF49H12.4*::GFP::Linker::NMY-1)] was produced by microinjecting plasmids pLSR11 (*pF49H12.4*::GFP::Linker::NMY-1), pCJS04 (*pF49H12.4*::mCherry) and pmyo-2::mCherry.

wdEx1009 (*pF49H12.4*::GFP::Linker::MLC-4DD) [NC3283] was obtained by microinjection of plasmids pLSR17 (*pF49H12.4*::GFP::Linker::MLC-4), pCJS04 (*pF49H12.4*::mCherry) and *pmyo-2*::mCherry.

Molecular biology

pLSR11 (*pF49H12.4*::GFP::Linker::NMY-1::*unc-10* 3'UTR). We used the Clonetech in-fusion HD cloning kit (Cat # 638910) to build this plasmid. The *nmy-1* genomic region was amplified from pACP01 (*pF49H12.4*::NMY-1::mCherry) with overlapping regions corresponding to pCJS95 (*pF49H12.4*::GFP::CED-10::*unc-10* 3'UTR). We also PCR amplified pCJS95 with primers overlapping the *nmy-1* genomic sequences to swap CED-10 with NMY-1. We then used the NEB site-directed mutagenesis kit to insert a 24-nucleotide glycine rich linker (see Table 1) [67]. The resultant pLSR11 plasmid was sequenced to confirm that the linker was inserted between the GFP sequence and *nmy-1*. See Table 1 for primer sequences.

Constructing pLSR17 (*pF49H12.4*::GFP::Linker::MLC-4DD). We used the Clonetech in-fusion HD cloning kit (Cat # 638910) to construct this plasmid. The *mlc-4* genomic region was amplified from wild-type (N2) DNA using primers with overlapping adapters complementary to pLSR11 (*pF49H12.4*::GFP::Linker::NMY-1). pLSR11 was amplified with primers containing adapter sequences complementary to *mlc-4*. The amplified fragments were combined for the infusion cloning to replace *nmy-1* with *mlc-4*. We then used the NEB site directed mutagenesis kit to change MLC-4 codons for Serine 18 and Threonine 17 to nucleotide sequences that encode aspartatic acid (D). The resultant pLSR17 plasmid was confirmed by sequencing.

Confocal microscopy and image analysis. Animals were immobilized with 15 mM levamisole/ 0.05% tricaine and mounted on 2% agarose pads in M9 buffer as previously described [11]. Z stack images were collected using a Nikon TiE inverted fluorescent microscope equipped with an A1R point scanning confocal and a Plan Apo 40X, 1.3NA oil immersion objective or on a Leica TCS SP5 confocal microscope with a 40X or 63X objective. Z stacks were collected at either 0.5 or 1μm depth from the position of ventral nerve cord to the top of PVD cell body. Maximum projection images were collated with either LAS-AF (Leica) or with NIS elements software (Nikon). Dendrite length was measured using the line tool in Fiji/image J. Co-localization images were assembled using image J. Z stack images that were collected using the LAS-AF or NIS elements software was imported into ImageJ/Fiji for further analysis.

iSIM super-resolution imaging and analysis. Animals were immobilized with 0.4 mM levamisole and mounted on 10% agarose pads in M9 buffer. Z stack images were captured using a Hamamatsu sCMOS camera on a iSIM microscope (VisiTech International) equipped

Table 1.

Primer name	Primer sequences
myrunc-5 Vec. For.	CGGCCGCGGATAACAAATTTCA
myrunc-5 Vec. Rev.	GGATCCCATCCCGGGGAT
myrunc-5 Frag. For.	CCCGGGATGGGATCCATGggatcttctaagtctgctagcAAAC
myrunc-5 Frag. Rev.	TGTTATCCGCGGCCGCTATTTGTATAGTTCATCCATGCCATGTG
nmy-1 linker F1	GGATGCCCCTCCgtacagctcgtccatg
nmy-1 linker R1	GCAGGGGGAGGTGATGGGTGACCTGCAGTAC
mlc-4DD F1	CATGTTCGATCAGGCTCAAATTCAAG
mlc-4DD R1	GCGAACACATTGTCATCGGCTCTTTG
mlc-4 Vec. For.	GGATAACAAATTTCTATGTTTTTGTTTGTTTTTTGTCTTAATTACCA
mlc-4 Vec. Rev.	ACCTCCCCCTGCGGATG
mlc-4 Frag. For.	TCCGCAGGGGGAGGTATGGCCTCCCGCAAAACC
mlc-4 Frag. Rev.	agaaatttgttatccTTAAGCCTCATCCTTGTCCTTGGTTCC

https://doi.org/10.1371/journal.pgen.1008228.t001

with a 100X, 1.45 NA objective. Images were deconvolved and processed using Metamorph and Fiji/ImageJ.

Spinning disk confocal microscopy. Animals were immobilized with 0.4mM levamisole and mounted on 10% agarose pads in M9 buffer. Volumes over time were captured using an automated TiE inverted fluorescence microscope platform with an X1 spinning disk head (Yokogawa) and DU-897 EM-CCD (Andor Technology), piezo-electric Z stage (Mad City Labs) and Apo TIRF 100x 1.49 NA oil immersion objective (Nikon Instruments, Inc.). Analysis of fluorescence intensity was accomplished using NIS-Elements and Fiji/Image J software.

Quantification of fluorescence intensity in growing vs. non-growing dendrites. L2-L3 larvae were immobilized with 0.4mM levamisole and mounted on 10% agarose pads in M9 buffer for imaging with the spinning disk confocal microscope. Z-stacks of PVD dendrites were imaged at either 1 min or 1.30 minute intervals with the 100X 1.49 NA oil immersion objective. PVD dendrites (2˚, 3˚ and 4˚) undergoing outgrowth with a succession of rapid extensions and retractions during the length of the time lapse videos were analyzed. NIS elements was used for measurements of LifeAct::GFP from a 1μm ROI at the tips of growing dendrites. In the same videos, fluorescence intensity was measured for an identical 1μm ROI of PVD branches (1˚, 2˚ and 3˚) that were not undergoing outgrowth. Fluorescence intensity measurements for the outgrowth and no-outgrowth datasets were normalized against the maximum overall LifeAct::GFP value (Fig 5).

Statistics. Student's t test was used for comparisons between 2 groups and ANOVA for comparisons between three or more groups with either Tukey posthoc or Bonferroni correction for multiple comparisons. Kolmogorov-Smirnov test was performed for comparisons between frequency distributions of 3˚ dendrite length and gaps between 3˚ dendrites (Figs 1C, 8F and 8G).

Supporting information

S1 Methods.
(DOCX)

S1 Fig. UNC-6/Netrin signaling mediates sister dendrite self-avoidance. (A-B) Representative images and tracings of PVD sensory neurons in wild-type (A) and *unc-6* (B) L4-stage larvae. PVD morphology was visualized with PVD::GFP or PVD::mCherry markers. PVD cell body marked with an asterisk. (A) 1˚, 2˚, 3˚ and 4˚ dendritic branches and single axon (blue arrowhead) are denoted. (B) Red arrowheads point to overlaps between adjacent 3˚ dendrites that failed to self-avoid in *unc-6* mutants. Scale bars are 5 μm. C) Summary of self-avoidance in 3˚ PVD dendrites denoting growth, contact and retraction. (D) Model of self-avoidance mechanism involving reciprocal contact-dependent repulsion mediated by UNC-6/Netrin and its receptors, UNC-40/DCC and UNC-5 [9].
(TIFF)

S2 Fig. Mutations in *unc-34/Ena/VASP* and *unc-73/Trio* disrupt PVD dendrite morphology. Quantification of 1˚ dendrite outgrowth and (B) number of 2˚ dendrites in wild-type, *unc-34*, *unc-73*, *wsp-1* and PVD::mCherry::UNC-34;*unc-34*. Defective 1˚ dendrites show altered alignment and/or extension defects. Mutations in *unc-34* and *unc-73* but not *wsp-1* result in defective 1˚ dendrite outgrowth and fewer 2˚ dendrites. Note that expression of UNC-34::mCherry in PVD restores 3˚ self-avoidance (Fig 3C) but does not rescue 1˚ and 2˚ dendritic defects which suggests that UNC-34 function could be required in other cell types for normal PVD 1˚ and 2˚ outgrowth, $^{*}p = 0.02$, $^{**}p = 0.003$, $^{***}p<0.001$, Fisher's exact and 2-way ANOVA with Tukey's correction for multiple comparison. (C) Representative images

of PVD morphological defects in an *unc-34* mutant. Note premature termination of 1˚ dendrites (red arrowheads). (D) Representative image and drawing of PVD branching defects in a *tiam-1/GEF* mutant at the L4 stage. Scale bars are 10 μm. Mutant alleles are *unc-34(gm104)*, *unc-73(rh40)*, *wsp-1 (gm324)* and *tiam-1(tm1556)*.
(TIFF)

S3 Fig. Localization and trafficking of PVD:: mCherry::UNC-34 puncta in PVD using Airy Scan and TIRF microscopy. (A) Zeiss Airyscan images of PVD simultaneously labeled with PVD::LifeAct::GFP (green) and PVD::mCherry::UNC-34 (Magenta). Merge shown on right. Insets denote PVD dendrites (B). White arrows indicate 2˚, 3˚, and 4˚ dendrites. Scale bar is 10 μm.
(TIFF)

S4 Fig. Actin dynamics during dendrite self-avoidance. Schematic (left) of adjacent 3˚ dendrites and representative time lapse series (35 sec intervals) of PVD::mCherry and PVD::LifeAct::GFP in 3˚ dendrites showing self-avoidance response (Condition 1). Point of contact is indicated by an asterisk and period of contact denoted with dashed blue outline. Scale bar is 10 μm. (B) Schematic depicting ROIs for fluorescence intensity measurements at the tips of adjacent (left vs right) 3˚ dendrites that undergo contact and at an adjacent non-contact (control) region. (C) Graphical representation of the change in fluorescence intensity at each time point vs that of 2 time intervals (t-2) before contact (t = 0); Measurements were normalized to fluorescence intensity at t-2 or (F_{t-2}) [39]. Normalized fluorescence intensity values were plotted against time (min) for LifeAct::GFP contacting 3˚ dendrites vs non-contact, and were compared by 2-way Anova with Bonferonni correction, p = 0.54 (N = 14). (D) Time lapse series collected with 100X objective at 1–1.3 minute intervals (N = 8) (Condition 2). The values for LifeAct::GFP at contact vs non-contacting region of 3˚ dendrites at each time-point were compared by 2-way Anova with Bonferonni correction, p = 0.74, NS (Not Significant).
(TIFF)

S5 Fig. Actin dynamics during dendrite self-avoidance. (A-D) Fluorescent intensity traces wild-type PVD dendrites during 3˚ dendrite self-avoidance. Fluorescent intensity measurements of PVD::LifeAct::GFP and PVD::mCherry were acquired at either 1 min (A-B) or 1.3 min (C-D) intervals from a 1μm region at the tips of the growing and contacting left and right 3˚ dendrites (Late L3-L4 animals). Measurements were normalized against the maximum intensity during a ~10 minute interval that includes at least one contact event. The gap between the left and right 3˚ dendrites undergoing contact was determined from the cytoplasmic mCherry signal and plotted against time. The period of contact (vertical shading) corresponds to a minimum value for the gap (0–0.14μm) between contacting left and right 3˚ dendrites. (E) Representation of 3˚ dendrites with color schemes to indicate left and right 3˚ dendrites and 1μm regions quantified.
(TIFF)

S1 Movie. Time-lapse video representing the dynamic movement of 3˚ dendrites in a wild-type background. Images of PVD::GFP were recorded (late L3-early L4) at 15 sec intervals with a 100X objective in a Nikon spinning disk microscope (see Materials and Methods). The length of the video is 240 seconds. The movie was edited using NIS elements software with Bayes advanced denoising. Green arrowheads denote the tips of 3˚ dendrites. Scale bar is 25 μm.
(MP4)

S2 Movie. Time-lapse video of 3˚ dendrites in a PVD::MYR::UNC-5. Images of PVD::GFP in the PVD::MYR::UNC-5 strain were recorded (late L3-early L4) at 15 sec intervals with a

100X objective in a Nikon spinning disk microscope (see Materials and Methods). The entire length of the video is 12 minutes. Boxes denote tips of 3˚ dendrites showing limited outgrowth. The movie was edited using NIS elements software with Bayes advanced denoising. Scale bar is 10μm.
(MP4)

S3 Movie. Time-lapse video showing the dynamicity of LifeAct::GFP during in 3˚ PVD dendrites. Images of PVD::mCherry (left) and PVD::LifeAct::GFP (right) and were collected at 1.3 min intervals with a 100 X objective in a Nikon spinning disk microscope (see Materials and Methods). The entire length of the video is 60 minutes. The movie was edited using NIS elements with automatic deconvolution. Scale bar is 5 μm. Spherical objects are autofluorescent granules.
(MP4)

S4 Movie. Time-lapse video showing dynamic LifeAct::GFP signal in 3˚ sister dendrites. Images of PVD::mCherry (left) and PVD::LifeAct::GFP (right) and were collected at 1.3 min intervals with a 100 X objective in a Nikon spinning disk microscope (see Materials and Methods). The length of the video is 60 minutes. The movie was edited using NIS elements with automatic deconvolution. Arrows track 3˚ dendrites undergoing contact and retraction. Scale bar is 5 μm.
(MP4)

S1 Data. The excel sheets include the self-avoidance score sheets for the various mutant backgrounds and the fluorescent intensity calculations in a PVD::LifeAct::GFP background at tips of 3˚ dendrites undergoing self-avoidance.
(ZIP)

Acknowledgments

We thank C. Bargmann, K. Shen, J. Plastino, Dr. T.J. Kubiseski, E. Lundquist, P. Mains and H. Buelow for strains and reagents. We thank Chun-Liang Pan and Chien-Po Liao for sharing their work, reagents and advice prior to publication, Dylan Burnette and members of his laboratory, Aidan Fenix and Nilay Taneja, for helpful suggestions and members of the Miller lab for comments on the manuscript. Spinning disk images were obtained in the Nikon Center of Excellence at Vanderbilt University. Airyscan images were obtained in the Vanderbilt Cell Imaging Shared Resource (CISR). We thank Fernando Delaville and Ralph Bauer from BioVision Technologies for their help in acquiring time-lapse movies and images on the iSIM microscope. Some of the strains used in this work were provided by the *C. elegans* Genetics Center. L.S., C.J.S and J.D.W. performed experiments with advice from D.M.M., M.J.T. provided imaging expertise and advice; B.A.M helped with spinning disk imaging and edited videos, L.S. and D.M.M. wrote the paper with input from coauthors.

Author Contributions

Conceptualization: Lakshmi Sundararajan, Cody J. Smith, Joseph D. Watson, Bryan A. Millis, Matthew J. Tyska, David M. Miller, III.

Data curation: Lakshmi Sundararajan, Cody J. Smith, Joseph D. Watson, David M. Miller, III.

Formal analysis: Lakshmi Sundararajan, Cody J. Smith, Bryan A. Millis, Matthew J. Tyska, David M. Miller, III.

Funding acquisition: David M. Miller, III.

Investigation: Lakshmi Sundararajan, Cody J. Smith, Joseph D. Watson, David M. Miller, III.

Methodology: Lakshmi Sundararajan, Cody J. Smith, David M. Miller, III.

Project administration: David M. Miller, III.

Resources: Lakshmi Sundararajan, David M. Miller, III.

Supervision: Matthew J. Tyska, David M. Miller, III.

Validation: Lakshmi Sundararajan, Cody J. Smith, Bryan A. Millis, Matthew J. Tyska, David M. Miller, III.

Visualization: Lakshmi Sundararajan, Cody J. Smith, Joseph D. Watson, Bryan A. Millis, Matthew J. Tyska, David M. Miller, III.

Writing – original draft: Lakshmi Sundararajan.

Writing – review & editing: Lakshmi Sundararajan, Cody J. Smith, Joseph D. Watson, Bryan A. Millis, Matthew J. Tyska, David M. Miller, III.

References

1. Delandre C, Amikura R, Moore AW. Microtubule nucleation and organization in dendrites. cc. 2016; 15: 1685–1692. https://doi.org/10.1080/15384101.2016.1172158 PMID: 27097122
2. Jan YN, Jan LY. Branching out: mechanisms of dendritic arborization. Nat Rev Neurosci. 2010; 11: 316–328. https://doi.org/10.1038/nrn2836 PMID: 20404840
3. Konietzny A, Bär J, Mikhaylova M. Dendritic Actin Cytoskeleton: Structure, Functions, and Regulations. Front Cell Neurosci. 2017; 11: 147. https://doi.org/10.3389/fncel.2017.00147 PMID: 28572759
4. Grueber WB, Sagasti A. Self-avoidance and tiling: Mechanisms of dendrite and axon spacing. Cold Spring Harb Perspect Biol. 2010; 2: a001750–a001750. https://doi.org/10.1101/cshperspect.a001750 PMID: 20573716
5. Fuerst PG, Bruce F, Tian M, Wei W, Elstrott J, Feller MB, et al. DSCAM and DSCAML1 function in self-avoidance in multiple cell types in the developing mouse retina. Neuron. 2009; 64: 484–497. https://doi.org/10.1016/j.neuron.2009.09.027 PMID: 19945391
6. Lefebvre JL, Kostadinov D, Chen WV, Maniatis T, Sanes JR. Protocadherins mediate dendritic self-avoidance in the mammalian nervous system. Nature. Nature Publishing Group; 2012; 488: 517–521. https://doi.org/10.1038/nature11305 PMID: 22842903
7. Matthews BJ, Kim ME, Flanagan JJ, Hattori D, Clemens JC, Zipursky SL, et al. Dendrite self-avoidance is controlled by Dscam. Cell. 2007; 129: 593–604. https://doi.org/10.1016/j.cell.2007.04.013 PMID: 17482551
8. Gibson DA, Tymanskyj S, Yuan RC, Leung HC, Lefebvre JL, Sanes JR, et al. Dendrite Self-Avoidance Requires Cell-Autonomous Slit/Robo Signaling in Cerebellar Purkinje Cells. Neuron. Elsevier Inc; 2014; 81: 1040–1056. https://doi.org/10.1016/j.neuron.2014.01.009 PMID: 24607227
9. Smith CJ, Watson JD, Vanhoven MK, Colón-Ramos DA, Miller DM III. Netrin (UNC-6) mediates dendritic self-avoidance. Nat Neurosci. 2012; 15: 731–737. https://doi.org/10.1038/nn.3065 PMID: 22426253
10. Albeg A, Smith CJ, Chatzigeorgiou M, Feitelson DG, Hall DH, Schafer WR, et al. C. elegans multi-dendritic sensory neurons: morphology and function. Mol Cell Neurosci. 2011; 46: 308–317. https://doi.org/10.1016/j.mcn.2010.10.001 PMID: 20971193
11. Smith CJ, O'Brien T, Treinin M, Miller DM III. Time-lapse imaging and cell-specific expression profiling reveal dynamic branching and molecular determinants of a multi-dendritic nociceptor in C. elegans. Developmental Biology. 2010; 345: 18–33. https://doi.org/10.1016/j.ydbio.2010.05.502 PMID: 20537990
12. Drees F, Gertler FB. Ena/VASP: proteins at the tip of the nervous system. Current Opinion in Neurobiology. 2008; 18: 53–59. https://doi.org/10.1016/j.conb.2008.05.007 PMID: 18508258
13. Goley ED, Welch MD. The ARP2/3 complex: an actin nucleator comes of age. Nat Rev Mol Cell Biol. 2006; 7: 713–726. https://doi.org/10.1038/nrm2026 PMID: 16990851
14. Takenawa T, Suetsugu S. The WASP-WAVE protein network: connecting the membrane to the cytoskeleton. Nat Rev Mol Cell Biol. 2007; 8: 37–48. https://doi.org/10.1038/nrm2069 PMID: 17183359

15. Steven R, Kubiseski TJ, Zheng H, Kulkarni S, Mancillas J, Ruiz Morales A, et al. UNC-73 activates the Rac GTPase and is required for cell and growth cone migrations in C. elegans. Cell. 1998; 92: 785–795. PMID: 9529254

16. Hu S, Pawson T, Steven RM. UNC-73/Trio RhoGEF-2 Activity Modulates Caenorhabditis elegans Motility Through Changes in Neurotransmitter Signaling Upstream of the GSA-1/G s Pathway. Genetics. 2011; 189: 137–151. https://doi.org/10.1534/genetics.111.131227 PMID: 21750262

17. Matsuo N, Hoshino M, Yoshizawa M, Nabeshima Y-I. Characterization of STEF, a guanine nucleotide exchange factor for Rac1, required for neurite growth. J Biol Chem. 2002; 277: 2860–2868. https://doi.org/10.1074/jbc.M106186200 PMID: 11707441

18. Demarco RS, Struckhoff EC, Lundquist EA. The Rac GTP exchange factor TIAM-1 acts with CDC-42 and the guidance receptor UNC-40/DCC in neuronal protrusion and axon guidance. PLoS Genetics. Public Library of Science; 2012; 8: e1002665. https://doi.org/10.1371/journal.pgen.1002665 PMID: 22570618

19. Krause M, Leslie JD, Stewart M, Lafuente EM, Valderrama F, Jagannathan R, et al. Lamellipodin, an Ena/VASP ligand, is implicated in the regulation of lamellipodial dynamics. Developmental Cell. 2004; 7: 571–583. https://doi.org/10.1016/j.devcel.2004.07.024 PMID: 15469845

20. Chang C, Adler CE, Krause M, Clark SG, Gertler FB, Tessier-Lavigne M, et al. MIG-10/lamellipodin and AGE-1/PI3K promote axon guidance and outgrowth in response to slit and netrin. Curr Biol. 2006; 16: 854–862. https://doi.org/10.1016/j.cub.2006.03.083 PMID: 16618541

21. Demarco RS, Lundquist EA. RACK-1 Acts with Rac GTPase Signaling and UNC-115/ abLIM in Caenorhabditiselegans Axon Pathfinding and Cell Migration. PLoS Genetics. 2010; 6: 1–17. https://doi.org/10.1371/journal.pgen.100121

22. Shakir MA, Jiang K, Struckhoff EC, Demarco RS, Patel FB, Soto MC, et al. The Arp2/3 activators WAVE and WASP have distinct genetic interactions with Rac GTPases in Caenorhabditis elegans axon guidance. Genetics. 2008; 179: 1957–1971. https://doi.org/10.1534/genetics.108.088963 PMID: 18689885

23. Levy-Strumpf N, Culotti JG. VAB-8, UNC-73 and MIG-2 regulate axon polarity and cell migration functions of UNC-40 in C. elegans. Nature Publishing Group. 2007; 10: 161–168. https://doi.org/10.1038/nn1835 PMID: 17237777

24. Tang LT, Díaz-Balzac CA, Rahman M, Ramirez-Suarez NJ, Salzberg Y, Lazaro-Pena MI, et al. TIAM-1/GEF can shape somatosensory dendrites independently of its GEF activity by regulating F-actin localization. eLife. 2019; 8: 507. https://doi.org/10.7554/eLife.38949 PMID: 30694177

25. Zou W, Dong X, Broederdorf TR, Shen A, Kramer DA, Shi R, et al. A Dendritic Guidance Receptor Complex Brings Together Distinct Actin Regulators to Drive Efficient F-Actin Assembly and Branching. Developmental Cell. 2018; 45: 362–375.e3. https://doi.org/10.1016/j.devcel.2018.04.008 PMID: 29738713

26. Oren-Suissa M, Hall DH, Treinin M, Shemer G, Podbilewicz B. The fusogen EFF-1 controls sculpting of mechanosensory dendrites. Science. 2010; 328: 1285–1288. https://doi.org/10.1126/science.1189095 PMID: 20448153

27. Norris AD, Sundararajan L, Morgan DE, Roberts ZJ, Lundquist EA. The UNC-6/Netrin receptors UNC-40/DCC and UNC-5 inhibit growth cone filopodial protrusion via UNC-73/Trio, Rac-like GTPases and UNC-33/CRMP. Development. 2014; 141: 4395–4405. https://doi.org/10.1242/dev.110437 PMID: 25371370

28. Killeen M, Tong J, Krizus A, Steven R, Scott I, Pawson T, et al. UNC-5 function requires phosphorylation of cytoplasmic tyrosine 482, but its UNC-40-independent functions also require a region between the ZU-5 and death domains. Developmental Biology. 2002; 251: 348–366. PMID: 12435363

29. Lai Wing Sun K, Correia JP, Kennedy TE. Netrins: versatile extracellular cues with diverse functions. Development. The Company of Biologists Limited; 2011; 138: 2153–2169. https://doi.org/10.1242/dev.044529 PMID: 21558366

30. Maniar TA, Kaplan M, Wang GJ, Shen K, Wei L, Shaw JE, et al. UNC-33 (CRMP) and ankyrin organize microtubules and localize kinesin to polarize axon-dendrite sorting. Nat Neurosci. Nature Publishing Group; 2011; 15: 48–56. https://doi.org/10.1038/nn.2970 PMID: 22101643

31. Chang C, Yu TW, Bargmann CI, Tessier-Lavigne M. Inhibition of netrin-mediated axon attraction by a receptor protein tyrosine phosphatase. Science. American Association for the Advancement of Science; 2004; 305: 103–106. https://doi.org/10.1126/science.1096983 PMID: 15232111

32. Gitai Z, Yu TW, Lundquist EA, Tessier-Lavigne M, Bargmann CI. The netrin receptor UNC-40/DCC stimulates axon attraction and outgrowth through enabled and, in parallel, Rac and UNC-115/AbLIM. Neuron. 2003; 37: 53–65. PMID: 12526772

33. Withee J, Galligan B, Hawkins N, Garriga G. Caenorhabditis elegans WASP and Ena/VASP proteins play compensatory roles in morphogenesis and neuronal cell migration. Genetics. 2004; 167: 1165–1176. https://doi.org/10.1534/genetics.103.025676 PMID: 15280232

34. Fleming T, Chien S-C, Vanderzalm PJ, Dell M, Gavin MK, Forrester WC, et al. The role of C. elegans Ena/VASP homolog UNC-34 in neuronal polarity and motility. Developmental Biology. 2010; 344: 94–106. https://doi.org/10.1016/j.ydbio.2010.04.025 PMID: 20452341

35. Chen C-H, Hsu H-W, Chang Y-H, Pan C-L. Adhesive L1CAM-Robo Signaling Aligns Growth Cone F-Actin Dynamics to Promote Axon-Dendrite Fasciculation in C. elegans. Developmental Cell. 2019; 48: 215–228.e5. https://doi.org/10.1016/j.devcel.2018.10.028 PMID: 30555000

36. Ramirez-Suarez NJ, Belalcazar HM, Salazar CJ, Beyaz B, Raja B, Nguyen KCQ, et al. Axon-Dependent Patterning and Maintenance of Somatosensory Dendritic Arbors. Developmental Cell. 2019; 48: 229–244.e4. https://doi.org/10.1016/j.devcel.2018.12.015 PMID: 30661986

37. Applewhite DA, Barzik M, Kojima S-I, Svitkina TM, Gertler FB, Borisy GG. Ena/VASP proteins have an anti-capping independent function in filopodia formation. Molecular Biology of the Cell. 2007; 18: 2579–2591. https://doi.org/10.1091/mbc.E06-11-0990 PMID: 17475772

38. Gates J, Mahaffey JP, Rogers SL, Emerson M, Rogers EM, Sottile SL, et al. Enabled plays key roles in embryonic epithelial morphogenesis in Drosophila. Development. 2007; 134: 2027–2039. https://doi.org/10.1242/dev.02849 PMID: 17507404

39. Liao C-P, Li H, Lee H-H, Chien C-T, Pan C-L. Cell-Autonomous Regulation of Dendrite Self-Avoidance by the Wnt Secretory Factor MIG-14/Wntless. Neuron. 2018; 98: 320–334.e6. https://doi.org/10.1016/j.neuron.2018.03.031 PMID: 29673481

40. Zhang W, Wu Y, Du L, Tang DD, Gunst SJ. Activation of the Arp2/3 complex by N-WASp is required for actin polymerization and contraction in smooth muscle. Am J Physiol, Cell Physiol. 2005; 288: C1145–60. https://doi.org/10.1152/ajpcell.00387.2004 PMID: 15625304

41. Riedl J, Crevenna AH, Kessenbrock K, Yu JH, Neukirchen D, Bista M, et al. Lifeact: a versatile marker to visualize F-actin. Nat Meth. 2008; 5: 605–607. https://doi.org/10.1038/nmeth.1220 PMID: 18536722

42. Smith CJ. Morphological and molecular characterization of somatosensory neurogenesis [Internet]. 2012. pp. 1–279. Available: http://login.proxy.library.vanderbilt.edu/login?url = http://search.proquest.com/docview/1627158315?accountid=14816

43. Piekny AJ, Mains PE. Rho-binding kinase (LET-502) and myosin phosphatase (MEL-11) regulate cytokinesis in the early Caenorhabditis elegans embryo. J Cell Sci. 2002; 115: 2271–2282. PMID: 12006612

44. Vicente-Manzanares M, Ma X, Adelstein RS, Horwitz AR. Non-muscle myosin II takes centre stage in cell adhesion and migration. Nat Rev Mol Cell Biol. 2009; 10: 778–790. https://doi.org/10.1038/nrm2786 PMID: 19851336

45. Somlyo AP, Somlyo AV. Signal transduction and regulation in smooth muscle. Nature. 1994; 372: 231–236. https://doi.org/10.1038/372231a0 PMID: 7969467

46. Ono K, Ono S. Two distinct myosin II populations coordinate ovulatory contraction of the myoepithelial sheath in the Caenorhabditis elegans somatic gonad. Molecular Biology of the Cell. American Society for Cell Biology; 2016; 27: 1131–1142. https://doi.org/10.1091/mbc.E15-09-0648 PMID: 26864628

47. Schroeder NE, Androwski RJ, Rashid A, Lee H, Lee J, Barr MM. Dauer-Specific Dendrite Arborization in C. elegans Is Regulated by KPC-1/Furin. Current Biology. Elsevier Ltd; 2013; 23: 1527–1535. https://doi.org/10.1016/j.cub.2013.06.058 PMID: 23932402

48. Salzberg Y, Ramirez-Suarez NJ, Bülow HE. The Proprotein Convertase KPC-1/Furin Controls Branching and Self-avoidance of Sensory Dendrites in Caenorhabditis elegans. Chisholm AD, editor. PLoS Genetics. 2014; 10: e1004657–13. https://doi.org/10.1371/journal.pgen.1004657 PMID: 25232734

49. Dong X, Chiu H, Park YJ, Zou W, Zou Y, Özkan E, et al. Precise regulation of the guidance receptor DMA-1 by KPC-1/Furin instructs dendritic branching decisions. eLife. eLife Sciences Publications Limited; 2016; 5: 308. https://doi.org/10.7554/eLife.11008 PMID: 26974341

50. Liu OW, Shen K. The transmembrane LRR protein DMA-1 promotes dendrite branching and growth in C. elegans. Nat Neurosci. 2011. https://doi.org/10.1038/nn.2978 PMID: 22138642

51. Sun LO, Jiang Z, Rivlin-Etzion M, Hand R, Brady CM, Matsuoka RL, et al. On and off retinal circuit assembly by divergent molecular mechanisms. Science. 2013; 342: 1241974–1241974. https://doi.org/10.1126/science.1241974 PMID: 24179230

52. Pollitt AY, Insall RH. WASP and SCAR/WAVE proteins: the drivers of actin assembly. J Cell Sci. The Company of Biologists Ltd; 2009; 122: 2575–2578. https://doi.org/10.1242/jcs.023879 PMID: 19625501

53. Castellano F, Le Clainche C, Patin D, Carlier MF, Chavrier P. A WASp-VASP complex regulates actin polymerization at the plasma membrane. EMBO J. 2001; 20: 5603–5614. https://doi.org/10.1093/emboj/20.20.5603 PMID: 11598004

54. Chen XJ, Squarr AJ, Stephan R, Chen B, Higgins TE, Barry DJ, et al. Ena/VASP proteins cooperate with the WAVE complex to regulate the actin cytoskeleton. Developmental Cell. 2014; 30: 569–584. https://doi.org/10.1016/j.devcel.2014.08.001 PMID: 25203209

55. Havrylenko S, Noguera P, Abou-Ghali M, Manzi J, Faqir F, Lamora A, et al. WAVE binds Ena/VASP for enhanced Arp2/3 complex-based actin assembly. Molecular Biology of the Cell. American Society for Cell Biology; 2015; 26: 55–65. https://doi.org/10.1091/mbc.E14-07-1200 PMID: 25355952

56. Colavita A, Culotti JG. Suppressors of ectopic UNC-5 growth cone steering identify eight genes involved in axon guidance in Caenorhabditis elegans. Developmental Biology. 1998; 194: 72–85. https://doi.org/10.1006/dbio.1997.8790 PMID: 9473333

57. Bashaw GJ, Kidd T, Murray D, Pawson T, Goodman CS. Repulsive axon guidance: Abelson and Enabled play opposing roles downstream of the roundabout receptor. Cell. 2000; 101: 703–715. PMID: 10892742

58. McConnell RE, Edward van Veen J, Vidaki M, Kwiatkowski AV, Meyer AS, Gertler FB. A requirement for filopodia extension toward Slit during Robo-mediated axon repulsion. The Journal of Cell Biology. 2016; 213: 261–274. https://doi.org/10.1083/jcb.201509062 PMID: 27091449

59. Hung R-J, Terman JR. Extracellular inhibitors, repellents, and semaphorin/plexin/MICAL-mediated actin filament disassembly. Cytoskeleton (Hoboken). John Wiley & Sons, Inc; 2011; 68: 415–433. https://doi.org/10.1002/cm.20527 PMID: 21800438

60. Lin C, Espreafico E, Mooseker M, Forscher P. Myosin drives retrograde F-actin flow in neuronal growth cones. Neuron. 1996; 16: 769–782. PMID: 8607995

61. Mitchison TJ, Cramer LP. Actin-based cell motility and cell locomotion. Cell. 1996; 84: 371–379. PMID: 8608590

62. Medeiros NA, Burnette DT, Forscher P. Myosin II functions in actin-bundle turnover in neuronal growth cones. Nat Cell Biol. 2006; 8: 215–226. https://doi.org/10.1038/ncb1367 PMID: 16501565

63. Murray A, Naeem A, Barnes SH, Drescher U, Guthrie S. Slit and Netrin-1 guide cranial motor axon pathfinding via Rho-kinase, myosin light chain kinase and myosin II. Neural Dev. 2010; 5: 16. https://doi.org/10.1186/1749-8104-5-16 PMID: 20569485

64. Brown JA, Wysolmerski RB, Bridgman PC. Dorsal root ganglion neurons react to semaphorin 3A application through a biphasic response that requires multiple myosin II isoforms. Molecular Biology of the Cell. 2009; 20: 1167–1179. https://doi.org/10.1091/mbc.E08-01-0065 PMID: 19109430

65. Brown JA, Bridgman PC. Disruption of the cytoskeleton during Semaphorin 3A induced growth cone collapse correlates with differences in actin organization and associated binding proteins. Devel Neurobio. 2009; 69: 633–646. https://doi.org/10.1002/dneu.20732 PMID: 19513995

66. Gallo G. RhoA-kinase coordinates F-actin organization and myosin II activity during semaphorin-3A-induced axon retraction. J Cell Sci. 2006; 119: 3413–3423. https://doi.org/10.1242/jcs.03084 PMID: 16899819

67. Fenix AM, Taneja N, Buttler CA, Lewis J, Van Engelenburg SB, Ohi R, et al. Expansion and concatenation of non-muscle myosin IIA filaments drive cellular contractile system formation during interphase and mitosis. Molecular Biology of the Cell. 2016; 27: 1465–1478. https://doi.org/10.1091/mbc.E15-10-0725 PMID: 26960797

68. Shutova MS, Spessott WA, Giraudo CG, Svitkina T. Endogenous species of mammalian nonmuscle myosin IIA and IIB include activated monomers and heteropolymers. Curr Biol. 2014; 24: 1958–1968. https://doi.org/10.1016/j.cub.2014.07.070 PMID: 25131674

69. Shutova M, Yang C, Vasiliev JM, Svitkina T. Functions of nonmuscle myosin II in assembly of the cellular contractile system. Parsons M, editor. PLoS ONE. Public Library of Science; 2012; 7: e40814. https://doi.org/10.1371/journal.pone.0040814 PMID: 22808267

70. Nithianandam V, Chien C-T. Actin blobs preFig dendrite branching sites. The Journal of Cell Biology. 2018; 217: 3731–3746. https://doi.org/10.1083/jcb.201711136

71. Díaz-Balzac CA, Rahman M, Lazaro-Pena MI, Martin Hernandez LA, Salzberg Y, Aguirre-Chen C, et al. Muscle- and Skin-Derived Cues Jointly Orchestrate Patterning of Somatosensory Dendrites. Curr Biol. 2016; 26: 2379–2387. https://doi.org/10.1016/j.cub.2016.07.008 PMID: 27451901

72. Dong X, Liu OW, Howell AS, Shen K. An Extracellular Adhesion Molecule Complex Patterns Dendritic Branching and Morphogenesis. Cell. 2013; 155: 296–307. https://doi.org/10.1016/j.cell.2013.08.059 PMID: 24120131

73. Salzberg Y, Díaz-Balzac CA, Ramirez-Suarez NJ, Attreed M, Tecle E, Desbois M, et al. Skin-Derived Cues Control Arborization of Sensory Dendritesin Caenorhabditis elegans. Cell. Elsevier Inc; 2013; 155: 308–320. https://doi.org/10.1016/j.cell.2013.08.058 PMID: 24120132

74. Zou W, Shen A, Dong X, Tugizova M, Xiang YK, Shen K. A multi-protein receptor-ligand complex underlies combinatorial dendrite guidance choices in C. elegans. eLife. eLife Sciences Publications Limited; 2016; 5: e18345. https://doi.org/10.7554/eLife.18345 PMID: 27705746

75. Luo L, Wen Q, Ren J, Hendricks M, Gershow M, Qin Y, et al. Dynamic encoding of perception, memory, and movement in a C. elegans chemotaxis circuit. Neuron. 2014; 82: 1115–1128. https://doi.org/10.1016/j.neuron.2014.05.010 PMID: 24908490